BIOLOGICAL APPLICATIONS OF TERAHERTZ TIME-DOMAIN ATTENUATED TOTAL REFLECTION SPECTROSCOPY

A THESIS SUBMITTED TO
THE GRADUATE SCHOOL OF NATURAL AND APPLIED SCIENCES
OF
MIDDLE EAST TECHNICAL UNIVERSITY

BY

MELİS GELGEÇ

IN PARTIAL FULFILLMENT OF THE REQUIREMENTS
FOR
THE DEGREE OF MASTER OF SCIENCE
IN
PHYSICS

AUGUST 2022

Approval of the thesis:

BIOLOGICAL APPLICATIONS OF TERAHERTZ TIME-DOMAIN ATTENUATED TOTAL REFLECTION SPECTROSCOPY

submitted by **MELİS GELGEÇ** in partial fulfillment of the requirements for the degree of **Master of Science** i**n Physics, Middle East Technical University** by,

Prof. Dr. Halil Kalıpçılar
Dean, Graduate School of **Natural and Applied Sciences** _____

Prof. Dr. Seçkin Kürkçüoğlu
Head of the Department, **Physics** _____

Prof. Dr. Hakan Altan
Supervisor, Physics**, METU** _____

Examining Committee Members:

Prof. Dr. Kıvanç Kamburoğlu
Dentistry, Ankara University _____

Prof. Dr. Hakan Altan
Physics, METU _____

Assoc. Prof. Dr. Alpan Bek
Physics, METU _____

Date: 25.08.2022

I hereby declare that all information in this document has been obtained and presented in accordance with academic rules and ethical conduct. I also declare that, as required by these rules and conduct, I have fully cited and referenced all material and results that are not original to this work.

Name Last name : Melis Gelgeç

Signature :

ABSTRACT

BIOLOGICAL APPLICATIONS OF TERAHERTZ TIME-DOMAIN ATTENUATED TOTAL REFLECTION SPECTROSCOPY

Gelgeç, Melis
Master of Science, Physics
Supervisor : Prof. Dr. Hakan ALTAN

August 2022, 80 pages

In this thesis, a Terahertz Attenuated Total Reflection Time Domain Spectroscopy (THz ATR-TDS) system was constructed to measure biological media. The constructed system driven by a Yb:doped mode-locked fiber laser had a limited bandwidth of about 0.3 THz. This bandwidth limited the analysis of various samples in the frequency domain. To overcome this limitation a method was developed so that the samples can be analyzed in the time-domain. Oral soft tissue samples collected were used in order to demonstrate that the THz ATR-TDS signals of the samples can be simulated using Inverse Fourier Transformation after analyzing the reference signals obtained without samples. Here, the refractive index of the soft tissue samples are estimated and used to model the frequency domain reference measurement after which the time-domain signals are obtained. The THz ATR-TDS measurements obtained from collected oral tissue samples are compared to simulated data and are shown to be in well agreement.

5 different types of oral tissue samples sliced to lay flat on the ATR prism surface provided by the Faculty of Dentistry of Ankara University in Ankara, Turkey were used in this study.

Due to the very high percentage of water contained in the biological samples, the refractive index of the all biological samples was assumed as $1.3818 \pm 0.0049i$ in

the spectral measurement range of the constructed system. Possible differences between this value and the actual value of the refractive indexes of the different samples are shown to be very small. Careful analysis of these differences can lead to a better estimation of the refractive index of the biological medium.

Keywords: Time Domain Terahertz Spectroscopy, Terahertz ATR Spectroscopy, Biological applications of Terahertz ATR spectroscopy, inverse Fourier transform analysis

ÖZ

ZAMANA BAĞLI ZAYIFLATILMIŞ TOPLAM YANSIMA TERAHERTZ SPEKTROSKOPİSİNİN BİYOLOJİK UYGULAMALARI

Gelgeç, Melis
Yüksek Lisans, Fizik
Tez Yöneticisi: Prof. Dr. Hakan Altan

Ağustos 2022, 80 sayfa

Bu tezde, biyolojik ortamı ölçmek için bir Terahertz Zayıflatılmış Toplam Yansıma Zaman Alanı Spektroskopisi (THz ATR-TDS) sistemi oluşturulmuştur. Yb:katkılı mod kilitli fiber kullanılarak yapılandırılmış sistem, yaklaşık 0.3 THz'lik sınırlı bir bant genişliğine sahipti. Bu bant genişliği, frekans alanındaki çeşitli örneklerin analizini sınırladı. Bu sınırlamanın üstesinden gelmek için, örneklerin zaman alanında analiz edilebilmesi için bir yöntem geliştirilmiştir. Numuneler olmadan elde edilen referans sinyalleri analiz edildikten sonra, numunelerin THz ATR-TDS sinyallerinin Ters Fourier Dönüşümü kullanılarak simüle edilebileceğini göstermek için ağızdan alınan yumuşak doku numuneleri kullanıldı. Burada, yumuşak doku örneklerinin kırılma indisi tahmin edilir ve zaman alan sinyallerinin elde edilmesinden sonra frekans alanı referans ölçümünü modellemek için kullanılır. Toplanan oral doku örneklerinden elde edilen THz ATR-TDS ölçümleri, simüle edilmiş verilerle karşılaştırılır ve iyi bir uyum içinde oldukları gösterilir.

Bu çalışmada Ankara Üniversitesi Diş Hekimliği Fakültesi tarafından sağlanan ATR prizma yüzeyine düz olacak şekilde dilimlenmiş 5 farklı tipte oral doku örneği kullanılmıştır.

Biyolojik numunelerde bulunan su oranının çok yüksek olması nedeniyle, oluşturulan sistemin spektral ölçüm aralığında tüm biyolojik numunelerin kırılma indisi $1.3818 \pm 0.0049i$ olarak kabul edilmiştir. Bu değer ile farklı örneklerin kırılma indekslerinin gerçek değeri arasındaki olası farkların çok küçük olduğu gösterilmiştir. Bu farklılıkların dikkatli analizi, biyolojik ortamın kırılma indisinin daha iyi tahmin edilmesine yol açabilir.

Anahtar Kelimeler: Terahertz Zamana Dayalı Spektroskopi, Terahertz Azalan Toplam İç Yansıma Spektroskopisi, Terahertz ATY Spektroskopisinin Biyolojik Uygulamaları,Ters Fourier Dönüşümü analizi

To my grandmother

ACKNOWLEDGMENTS

I would like to give special thanks to my supervisor Prof. Dr. Hakan Altan for his support throughout my master degree program. I would like to express my deepest gratitude to my husband Cenker Ergen for making the completion of this thesis possible. I could not have undertaken this journey without my brother Murat Gelgeç.I would like to express my sincere gratitude for my mother and father Nejla & Nail Gelgeç. I am extremely grateful for my lovely cousins Leyta &Erkan Gerçel for their endless support. I am deeply indebted to all of my friends for their moral supports. Special thanks to Gizem Gül Yatarkalkmaz, Gonca Ünder, Kübra Cerit, Eylül Öcal,Sercan Aslan for their outstanding efforts to help me complete this thesis. I also would like to thank to my cats Albus & Luna for their lovely companionship.

This study is sponsored by TUBITAK (under project number 119S623.)

TABLE OF CONTENTS

LIST OF FIGURES

FIGURES

LIST OF ABBREVIATIONS

ATR	: Attenuated Total Reflection
EM	: Electromagnetic
EO	: Electro Optical
Fs	: Femtosecond
GaP	: Gallium Phosphide
GaSe	: Gallium Selenide
PCA	: Photo Conductive Antenna
THz	: Terahertz
ZnTe	: Zinc Telluride
Si	: Silicon
Yb	: Ytterbium
TIR	: Total Internal Reflection
LASER	: Light Amplification by Stimulated Emission of Radiation

CHAPTER 1

INTRODUCTION

Terahertz (THz) technologies have recently emerged as one of the most important areas of applied research, driven in large part by future imaging and spectroscopic applications. [1]

Terahertz radiation has a lot of advantages. It pierces almost all dielectric materials, including paper, plastics, coatings, and foams. It has properties that are unique to numerical organic compounds. It is safe since it is non-nucleonic and non-ionizing. These characteristics contribute to the rapid advancement of terahertz technology. [2]

1.1 Terahertz Radiation

Terahertz (THz) radiation is an electromagnetic radiation that is observed between the frequencies of 0.3 and 20 THz in the electromagnetic spectrum. 1012 Hz is equal to 1 THz. This range corresponds to wavelength 1 (30–3000 m), wavenumber k (3.3–334 cm1), period t (0.1–10 picoseconds), temperature T (4.8–478 K), and photon energy E (0.4–41 milli-electron volts). [3]

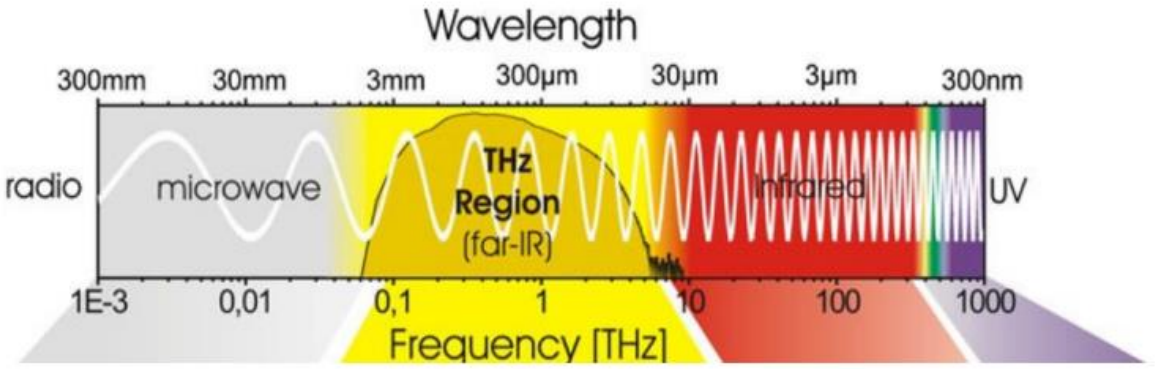

Figure 1.1 Three Region of the THz Radiation in Electromagnetic Spectrum [1]

Recent advancements in THz radiation generation systems have sparked interest in examining the interaction of radiation with biological molecules and tissue. [3]

It's worth noting that the energy level necessary to ionize biological molecules is several orders of magnitude lower than that of THz photons. Terahertz waves are therefore classified as non-ionizing radiation.[49] Because nonionizing and ionizing radiation have radically different effects on biological structures, this distinction is critical. The most notable distinction is that only ionizing radiation particles have sufficient energy to generate direct ionization effects in water and biomolecules. The biological structures are particularly vulnerable to these direct effects which makes Terahertz studies on biological tissues very important. [4]

Skin tissue is the best biological material for using THz-based methods since it allows you to get beyond some of the technique's inherent constraints, such as a small penetration depth (0.1 to 0.3 mm for the skin, on average). [5] This Small penetration depth is important here because water causes high THz absorption and this limits the penetration into the materials which contain water. [6]

1.2 Generation and Detection of Terahertz

Many technologies for generating and detecting terahertz (THz) radiation have been developed over the years and are continually being developed in many cases. [7][48] Inside the sections 1.2.1 and 1.2.2 most common methods for the generation and the detection of the terahertz radiation are explained.

1.2.1 THz Generation Methods

The most extensively used THz spectroscopy systems use femtosecond pulses generated by mode-locked lasers. The most common terahertz production methods are photoconductive emission and electro-optical rectification. [7]

A photo-conductive antenna (PCA) is made up of an antenna structure and a fast optically actuated switch. Metal electrodes on a semiconductor substrate are commonly used. The optical pulse is directed into the gap between two electrodes at femtoseconds. Electron–hole pairs will be created if this optical pulse has wavelength that is close to the semiconductor's bandgap. A DC voltage put between the metal electrodes produces an electric field in the gap, which accelerates the charges. On a picosecond time frame, these accelerated charges will be recaptured into the semiconductor band structure, bringing the system back to equilibrium.

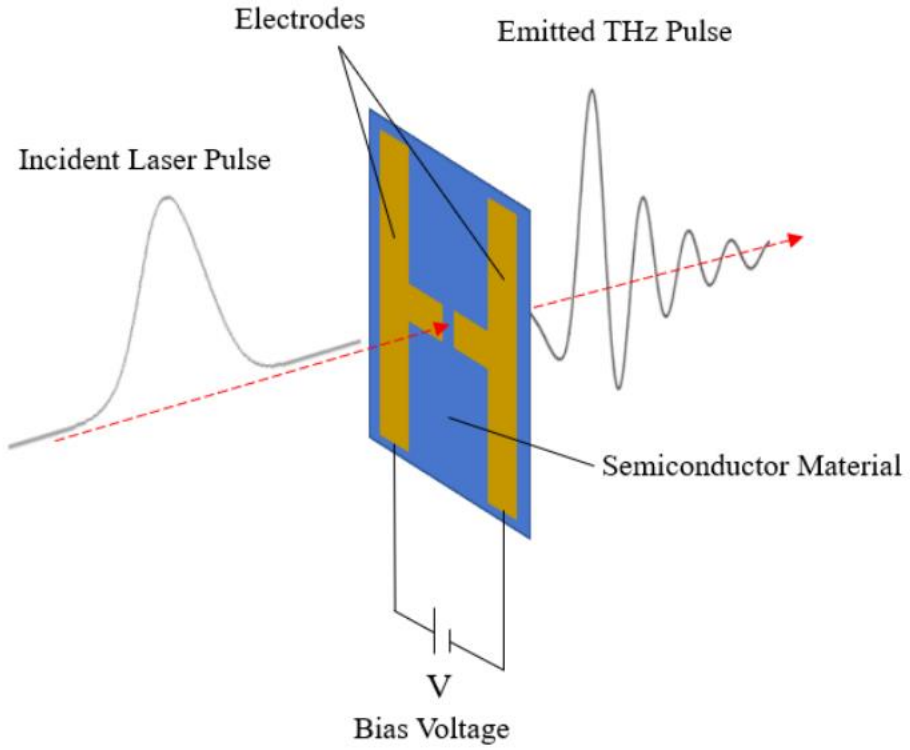

Figure 1.2 Terahertz Generation with PCA [8]

Crystals with nonlinear optical properties can also be used to create and detect THz radiation. Through the nonlinear medium, the femtosecond pulse enters and propagates. Induced polarization generates a THz electric field in the nonlinear medium. [9]

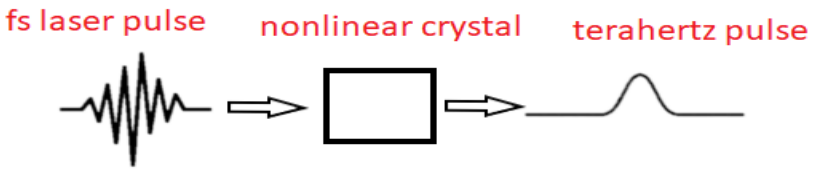

Figure 1.3 Terahertz Generation From Nonlinear Crystal

1.2.2 THz Detection Methods

PCAs and electro-optic (EO) sampling are the most used terahertz detection technologies. [10]

For the electro-optic sampling, the underpinning idea is the Pockels effect. The Pockels effect is defined as a change in the birefringence or refractive index of an optical medium made of an EO crystal. An applied electric field causes a change in birefringence. Variations in birefringence caused by the electric field of the signal are measured by a pair of photodetectors to detect the incident optical signal. [51]The optical medium is commonly made of materials like EO polymers, organic crystals, ZnTe, and GaAs.

The optical pulse's linear polarization state is changed to elliptical when it interacts with the THz pulse inside the EO crystal. A quarter wave plate (QWP) is used to regulate polarization after the EO medium has been applied. The elliptical polarization is then split in two parts using a Wollaston prism. Lastly, the balanced photodetector detects the intensity differences between these polarization components. The linear polarization of the optical pulse changes to circular when there isn’t an incident THz beam. That means, the intensity of separated perpendicular parts of circular polarization is equal. Considering that, balanced detector could not provide a signal because of the intensity differences. This indicates that the presence of a THz pulses within the medium effects directly the existence of signal, as the THz pulse alters the state of the optical pulse. Because of the Pockels effect, alteration in the polarization is proportional to the THz pulse’s electric field. As a result, the resulting signal will be proportional to the incident THz pulse's electric field. Figure 1.4 shows an illustration of this technique.

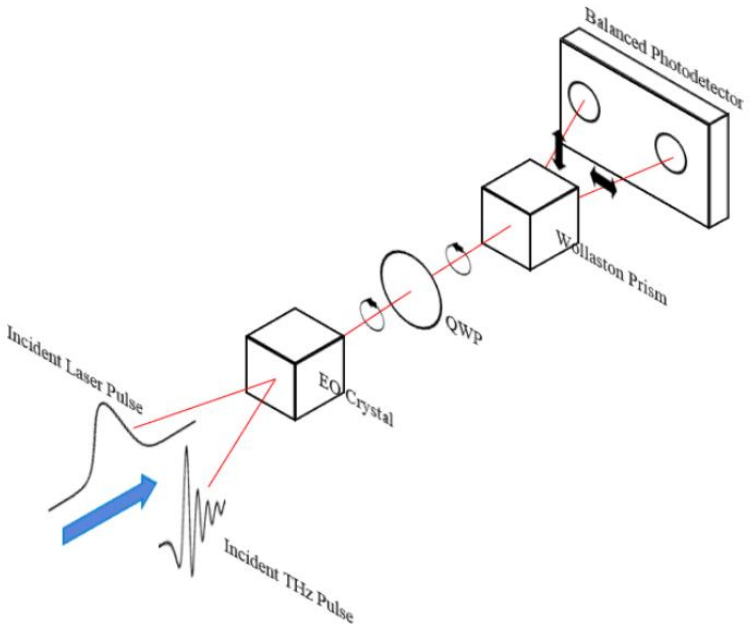

Figure 1.4 Terahertz Detection with Electro – Optic Method [8]

One of the most widely used emitters and detectors for THz radiation, as well as electrooptic (EO) crystals, is the PC antenna. The detection of terahertz with PCAs is similar to the generation of terahertz with PCA as well as the structures of the antennas. However, Electrodes being connected to an ammeter, not to the voltage source is a difference. Schematic of the PCA detection is shown in the below figure.

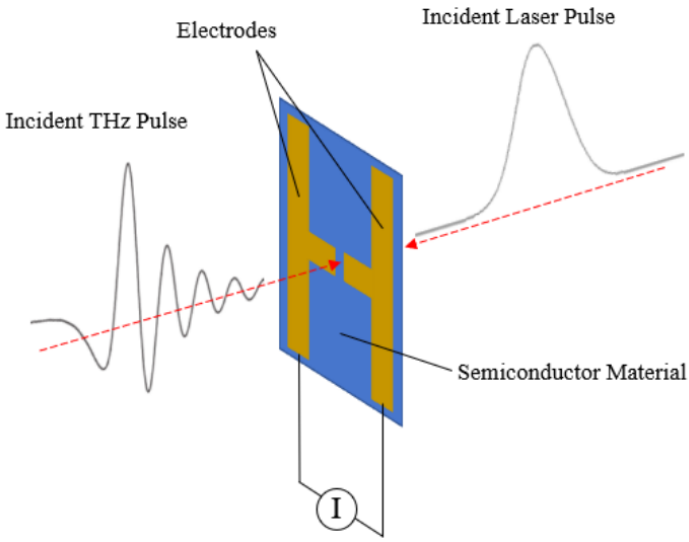

Figure 1.5 Terahertz Detection with PCA [8]

The physical technique of detection is also not different. It is, in actuality, the reverse of the generation technique. Inside the semiconductor material, the laser pulse focused on the antenna gap generates electron-hole pairs once more.[50] When a THz pulse strikes the antenna, the generated carriers are separated however in this method the electric field is caused by the THz beam. The presence of an electric field causes the acceleration of the carries, resulting in the generation of a current that has a magnitude proportional to the electric field of the THz wave. Even if the carrier pairs are formed, generation of the current does not place if there is no incident THz beam. The produced current is used to determine the intensity of the incident THz radiation. [9] [10] [11]

CHAPTER 2

THz TIME DOMAIN SPECTROSCOPY

Since the middle of the twentieth century, Fourier transform infrared (FTIR) spectroscopy has created new opportunities for spectroscopy study. The far-infrared area has piqued people's interest and continues to do so. [12]

The three key spectroscopy approaches in the terahertz region of the electromagnetic spectrum are terahertz time domain spectroscopy (THz-TDS), terahertz emission spectroscopy (TES), and time-resolved terahertz spectroscopy (TRTS). [13]

For optical characterisation of materials at terahertz frequencies, the THz-TDS technique, which was used in this thesis, is generally favoured above the ones stated previously.[45] One of the reasons for its popularity is that it can detect a wide variety of frequencies while being coherent. [14]

2.1 Time Domain Terahertz Spectroscopy System and It’s Properties

Terahertz time-domain spectroscopy (THz-TDS) is a powerful technique for determining a material's complex permittivity (or complex refractive index) and permeability in the far infrared.[47] Fast recordings at ambient temperature, high dynamic range, magnitude and phase recording, and broad bandwidth have all led to the rebirth of far-infrared studies. Owing to its superior performance and advantages-TDS is still utilized for the characterisation of many various materials and devices, such as anisotropic crystals, scattering heterogeneous materials, magneto-optical materials, metamaterials, and so on.

These systems work by measuring short electromagnetic pulse's temporal shape which may then be converted to the frequency domain via a Fourier transform.

This is an excellent demonstration of the Fourier transform's application in physics. The relevant spectrum enters the THz range when the pulse duration is of the order of picoseconds. As an outcome, the method integrates modern technology with the ultrashort pulse delivery and measurement requirements. Mode-locked ultrafast lasers can readily provide the required picosecond or, femtosecond pulses. The success of THz-TDS is due to the availability of very consistent and stable trains of repeating femtosecond laser pulses, which are commonly generated by fiber lasers. Furthermore, in contrast to microwaves or infrared domains, obtaining the temporal shape of electromagnetic pulses using time-equivalent methods necessitates a delay line where the optical components only need to move a few millimetres, which is technically simple. Generating infrared pulses (larger than a few terahertz) does, in fact, necessitate electromagnetic pulses of a few tens of femtoseconds. The quasi-optical setup in the microwave domain is quite large (considering the longer wavelengths), and the delay lines must be shifted over tens of centimetres, which can be difficult. [15][32]

The entire process can be stated as follows: a laser source generates pump and probe beams, a time delay is introduced between them, and sampling in time domain is obtained by employing the probe beam as a result of the introduced time delay. [33]

Using a wavelength and percentage compatible beam splitter, a pulse from an ultrafast laser source is divided into two distinct arms, known as the pump beam and probe beam. In most systems, this initial division is accomplished by 50:50 beam splitters, which approximately divide the incoming pulse evenly into two, however alternative percentages may be utilized depending on the design.

The THz generator receives the pump beam directly. However, the probe beam is first sent down a separate path known as a delay line, which is commonly built using a motorized stage and a retroreflector for temporal delay. The received THz signal is then captured by the THz detector. The time probe beam reaching the detector changes as the stage moves, so with each step, the probe beam scans a

different area of the generated THz beam and the detector detects THz. The entire sampling in time domain of the THz pulse generated by the emitter with regard to the time delay is achieved by moving down the delay line in a continuous manner. [46]The THz beam is caught as a function of time in this case. [38]

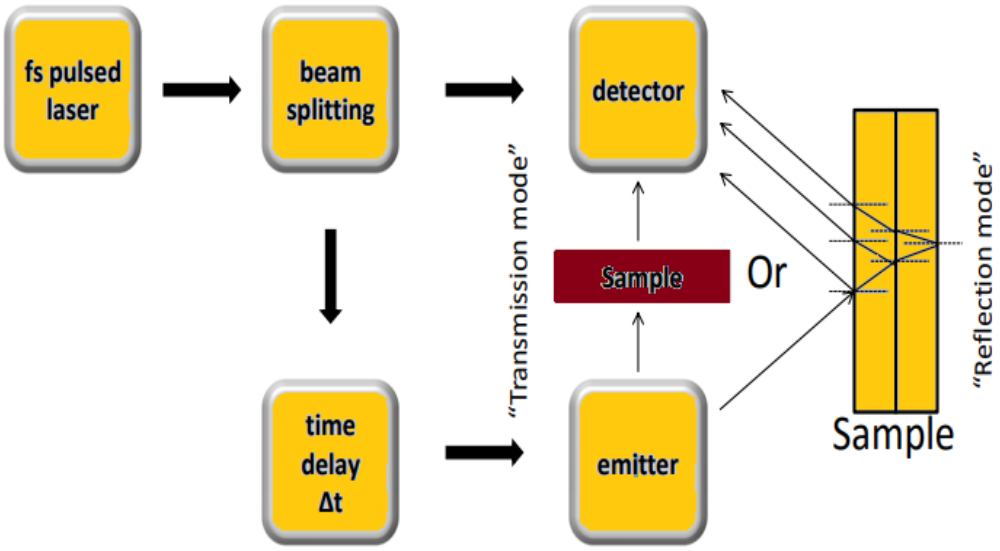

Figure 2.1 Typical THz Time Domain Spectroscopy System [16]

For the generation of the THz signal with PCA, a type of function generator that is chosen considering the antenna specifications can be used in order to supply an electric field so that the photocarriers which produced by beam striking onto the chip of PCA can be accelerated.

For the detection of the THz signal, a lock-in amplifier is compatible with the can be used to measure the signal. [17] [18] [8]

2.1.1 Time Domain Terahertz Spectroscopy Analysis

In this section, terahertz time domain spectroscopy analysis of a silicon sample is made using a THz-TDS system as explained in the above sections. Fourier Transform is applied to the recorded data from the THz-TDS system using the program called Origin Pro 8 firstly and Python secondly. Optical properties such as the refractive index, absorption coefficient, conductivity and even the sample thickness are analysed. For the further and more complex analyses, the main purpose of this thesis, Python will be used for the Fourier Transform and Inverse Fourier Transform analyses. With the simple analysis in this section, Origin Pro 8 results and Python results are compared and it is found that it is safe and accurate choice to continue with Python for the further and main Fourier transform analyses.

Below figures which are the Figure 2.2, the Figure 2.3 and the Figure 2.4 show the reference and sample (silicon) signal plots taken from a basic THz-TDS system with ZnTe crystal.

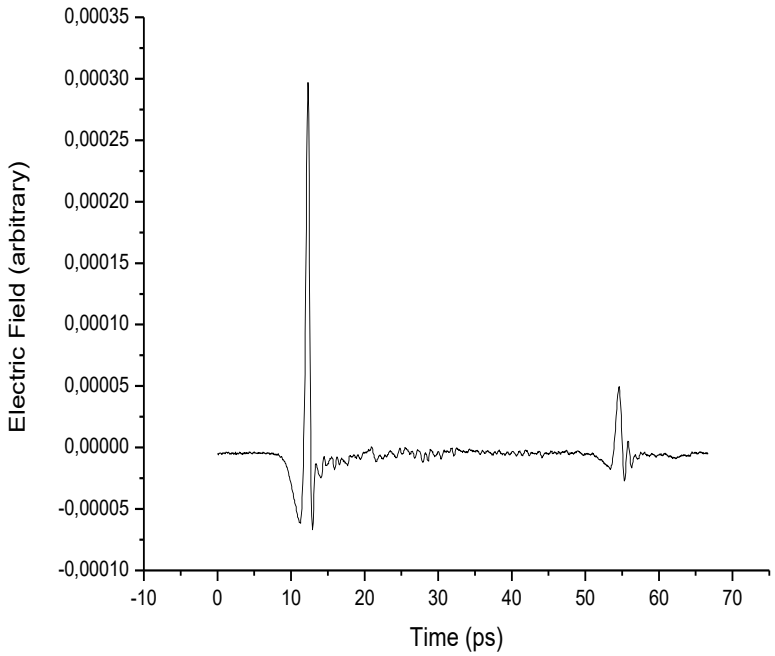

Figure 2.2 Reference Analysis (ZnTe Crystal with 2 mm Thickness)

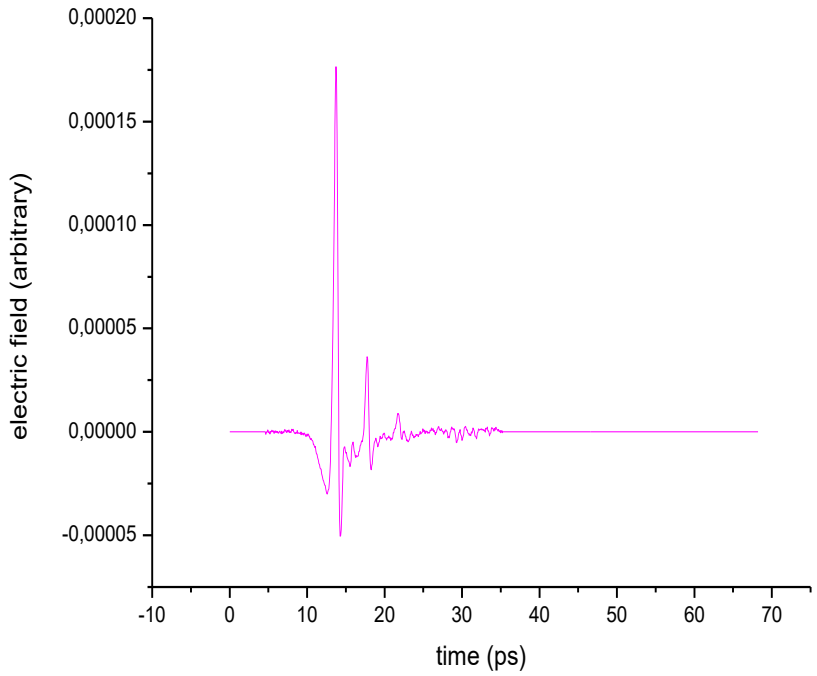

Figure 2.3 Sample Analysis (Silicon with 3.4 Refractive Index)

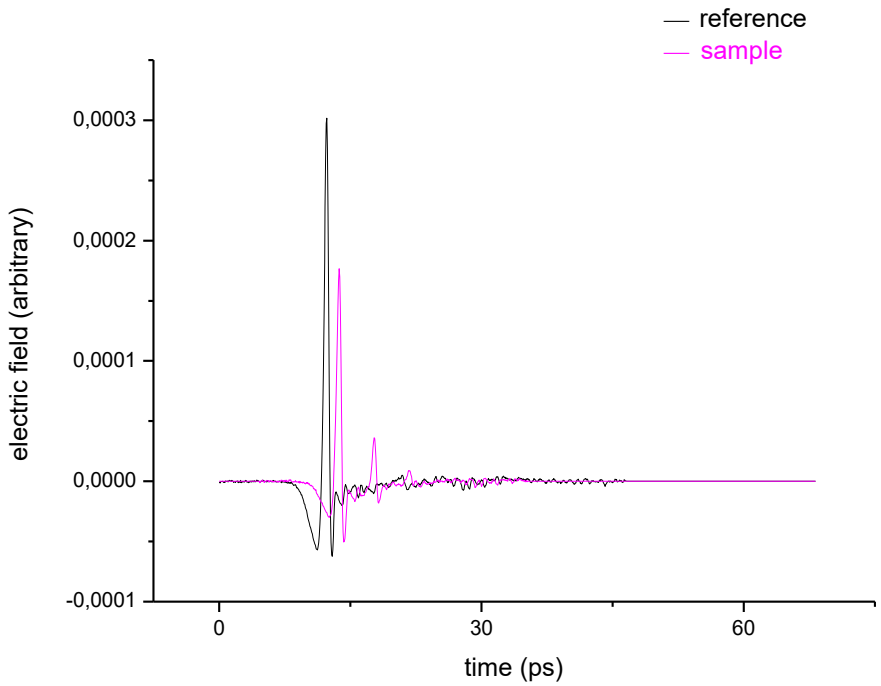

Figure 2.4 Sample and Reference Analysis Together

These graphs are electric field versus time graphs. And the electric field unit is arbitrary, not “volt”. The real value is not important here because when compared with reference data, units will be divided.

Disturbances on the right side of the graphs may be due to phase shifts and absorption. Interaction of terahertz pulse between some materials in the air or environment can cause these oscillations thus shape can change due to absorption of frequencies inside the pulse. Also, it could be the Rayleigh scattering however, for Rayleigh scattering being important here, it should be approximately in between 1 micron and 30 microns. So, this scattering can be important with a particle sample. And the second pulse on the graph1 and graph 2 is the reflection pulse (etalon effect) occurred when the pulse gets through crystal or sample due to internal reflection.

The refractive index of the ZnTe crystal can be find by using the equation $n = \frac{c \cdot \Delta t}{2d}$ Here “n” is the refractive index of the ZnTe crystal, “c” is the speed of light, “Δt” is the time difference between two peaks from the Figure 2.2 and “d” is the thickness.

$$\Delta t = 42.2976102 \text{ ps}$$

$$d = 2 \text{ mm}$$

then n is found as

$$n = 3.17$$

To find the thickness of the silicon the equation $n = \frac{c \cdot \Delta t}{2d}$ can be used where Δt is the time difference between two peaks from the Figure 2.3.

$$\Delta t = 3.99585 \text{ ps}$$

$$n = 3.4$$

then d is found as

d=176 microns

There is another way to calculate the thickness of the silicon with the equation

$$n = 1 + \frac{c \cdot \Delta t}{d}$$

Here "Δt" is the time difference between the first peak (reference) and the second peak (first peak of sample) from the Figure 2.4 "1" stands for the refractive index of air.

Δt=1.43ps

n=3.4

then thickness is found as,

d=178.75 microns

Thickness results are not exactly the same. When pulse gets through a material twice, some frequencies inside the pulse can be lost and peaks at the frequencies change so Δt is not exactly known. So, looking the differences between peaks from Figure 2.4 is better.

For the further analyses for the silicon sample Fourier transform is applied to the time-domain data and below optical analyses are obtained accordingly to the FFT results.

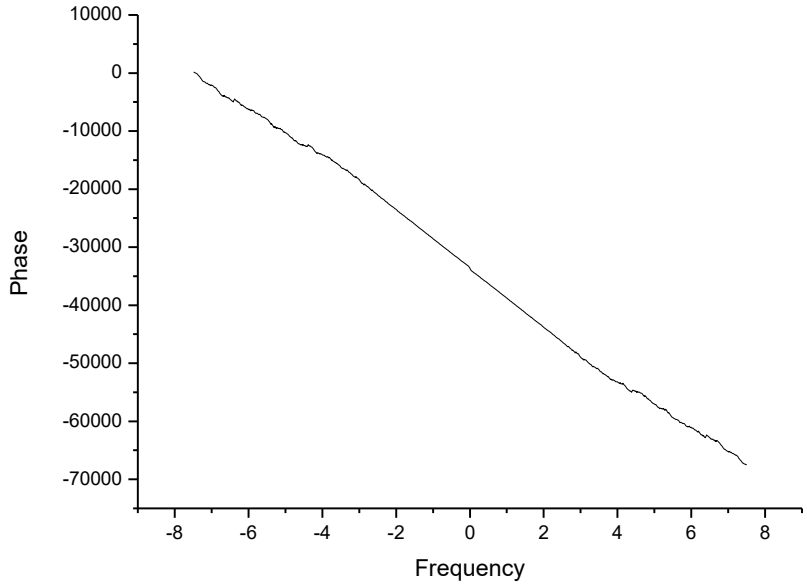

Figure 2.5 FFT Analysis for the Silicon

As seen in the Figure 2.5 point zero acts as if it is like a mirror. The part where the unwrap phase is linear has useful bandwidth (the part where signal to noise ratio is well). And the point where it breaks can be seen in the graph as above 2.5 THz.

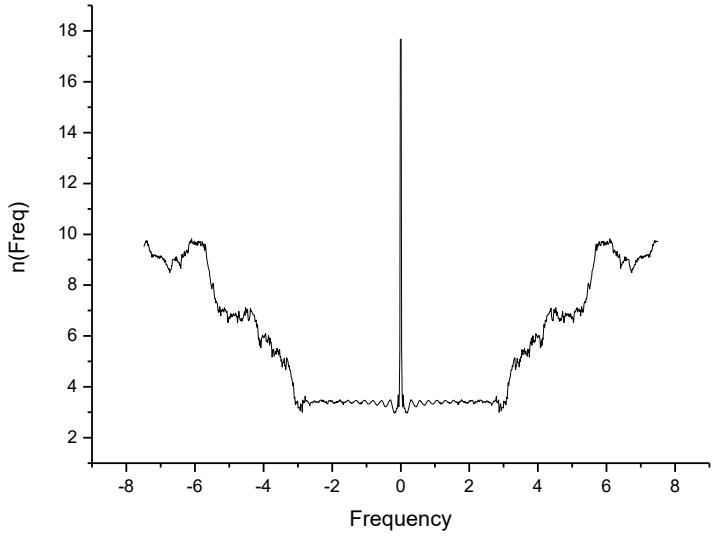

Figure 2.6 FFT Analysis for the Silicon

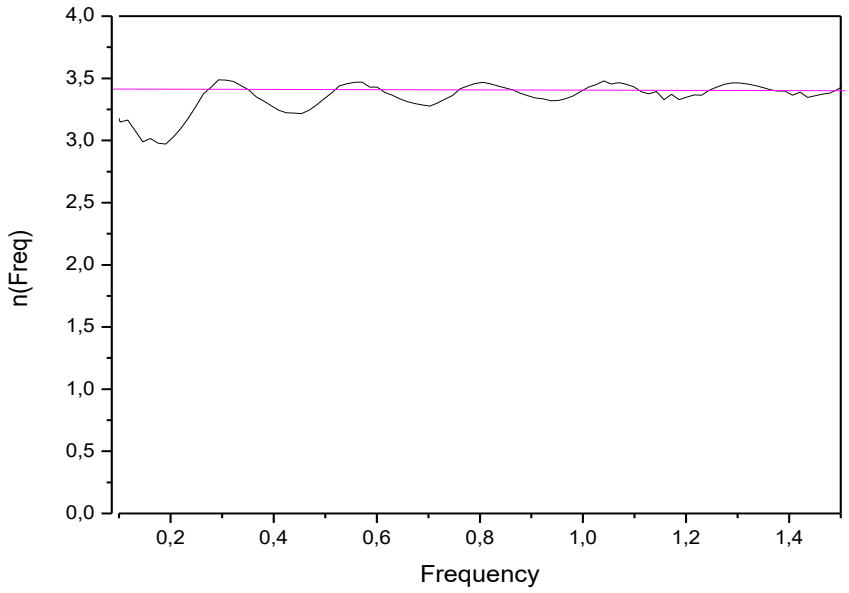

Figure 2.7 FFT Analysis for Silicon from 0 to 1.5 THz

As expected, “n” is around 3.40 for silicon.

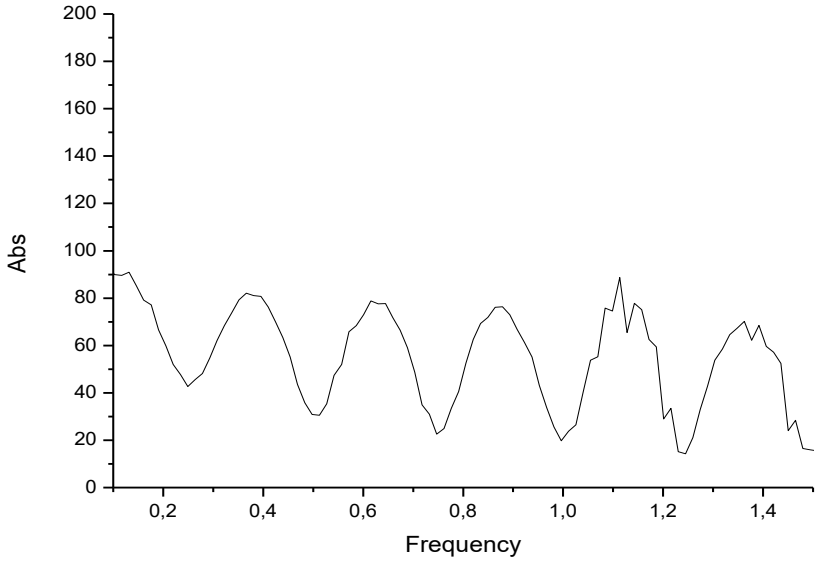

Figure 2.8 FFT Analysis for Silicon

From Figure 2.8 it can be seen that silicon has high resistivity from absorption coefficient graph.

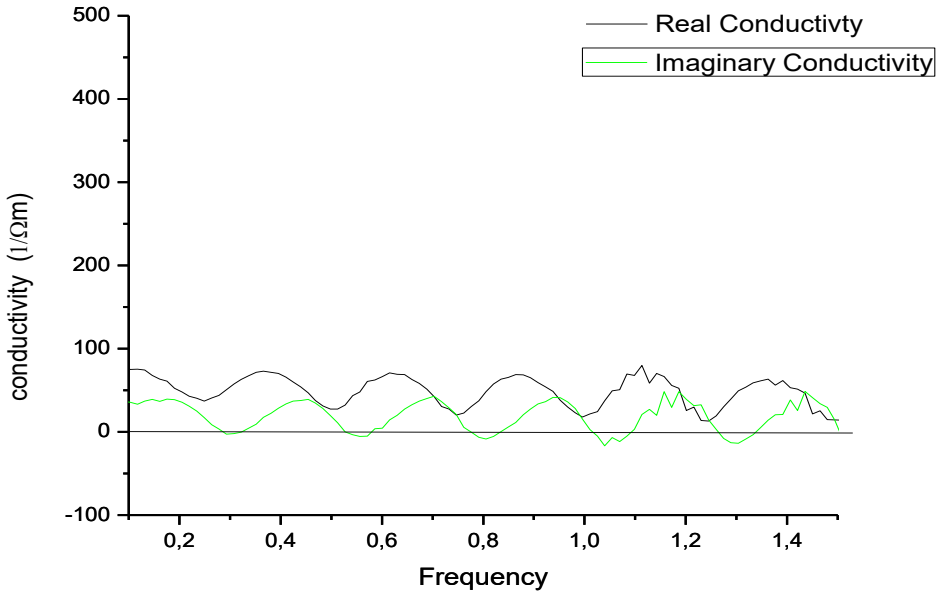

Figure 2.9 Conductivity for Silicon

Since the main purpose of this thesis suggests that using Inverse Fourier Transform, the sample pulse can be obtained, Inverse Fourier transform is applied to the frequency domain data to compare it with the original signal taken recorded from the system. The Figure 2.10 below shows that by applying Inverse Fourier Transform the original pulse can be detected.

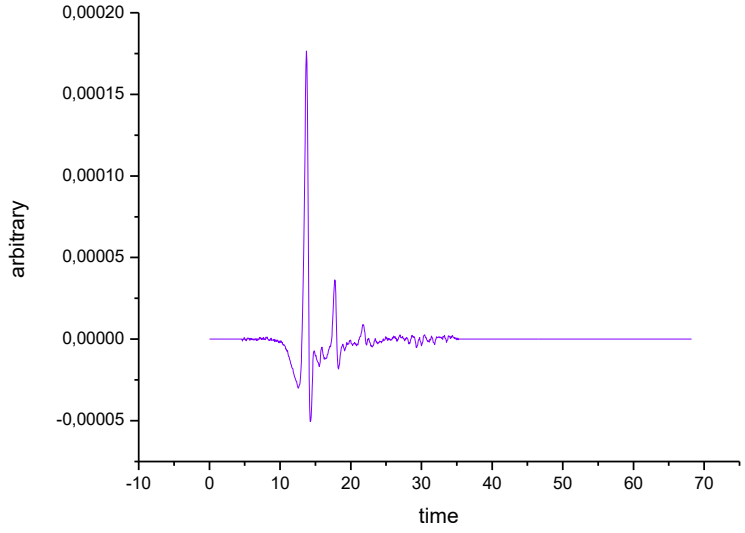

Figure 2.10 IFFT Analysis for Silicon

Before continuing for the THz-ATR system analysis using Python, Inverse Fourier Transform is applied using Python again to the frequency domain data to compare the proven result obtained from Origin Pro8.

Figure 2.11 below shows the IFFT Analysis for the Silicon using Python.

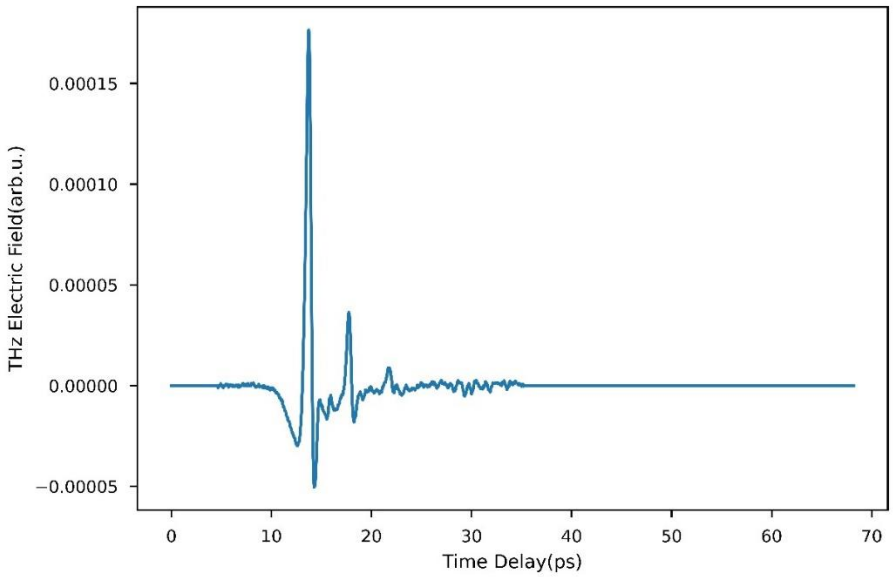

Figure 2.11 IFFT Analysis for Silicon using Python

As the graph shows, Python analysis result is the same with the Origin Pro 8 analysis result. From further on, FFT and IFFT analysis will be made using Python in this thesis.

2.2 Time Domain Terahertz ATR Spectroscopy

THz ATR-TDS system is fundamentally works with the same principles that are explained in previous sections. Although the experimental setups are similar, the theory behind the ATR spectroscopy is the most important distinction.

The properties of the evanescent wave resulting from total internal reflection are primarily used in the ATR spectroscopy system. The ATR crystal should be used and it should be made of a high refractive index material to meet the demand for total internal reflection. Along with Germanium, high-resistivity silicon is the most used material for ATR crystals. The optical geometry of the system determines the crystal form. When an electromagnetic wave is sent to the ATR crystal at the critical angle, the wave is refracted, and the wave subsequently reflects off the internal surface, generating an evanescent field close to the crystal–sample contact. [19]

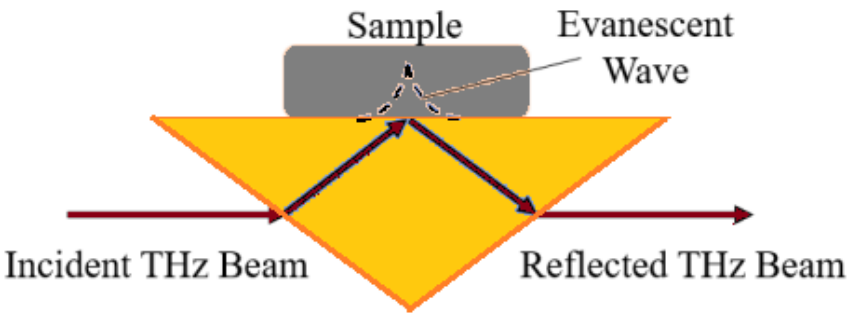

Figure 2.12 Prism of ATR

2.2.1 Ytterbium Doped Fiber Laser System

This system is working with the electro optic sampling technique which is explained in the first chapter.

The laser source of this system has wavelength around 1040 nm and pulse duration at 250 fs. GaBiAs based PCA is used for the generation of the THz. Guiding pulses through Si prism made possible by using two Teflon lenses which have the 5 cm radius and 1.5 f number. The radius of the focused beam at Si prism is 2.5 mm.The prism angle is 103.2 degree at the center of this focus. Thz pulses gathered after the internal reflection are determined on the ZnTe oriented crystal by electro optic method. Due to the phase difference occurred inside the crystal, frequency interval measured is restricted to the 0.5-0.6 THz.Measurement window of the system is up to 0.4 THz.

2.2.2 System Layout

A layout of the experimental system is shown in Figure 2.13 below, along with a list of its components.

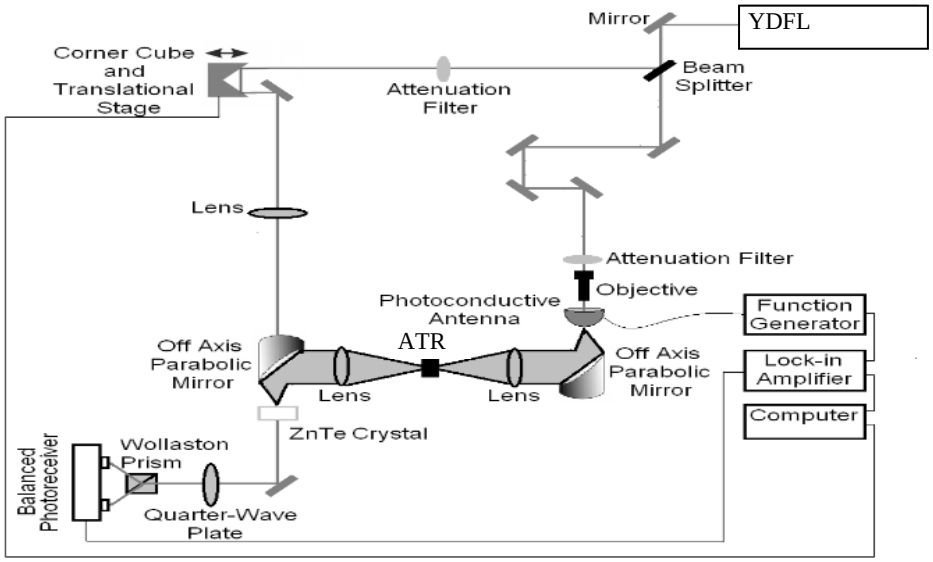

Figure 2.13 YDFL Pumped THz-ATR System Configuration

A) Main Arm

1) Ytterbium Doped mode-locked Fiber Laser
2) Attenuation Filter
3) Flat Mirrors
4) 50:50 Beam Splitter

B) THz Generation Arm

1) Objective
2) Function Generator: RIGOL DG2041A
3) PCA: Batop
4) Teflon Lenses

C) Measurement Section

1)Off Axis 90-degree Parabolic Mirrors

2) HRFZ-Si prism 54.85x21.74x35 mm. Base Angle: 103.2 degree.

3) Prism Holder

D) Detection Arm

1) ZnTe Crystal

2) QWP

3) Wollaston Prism

4) Balanced Photodetector

E) Data Acqusition

1) Stage Controller: Newport ESP301

2) Lock-in Amplifier: Standford Research Systems SR850 DSP

3) Computer

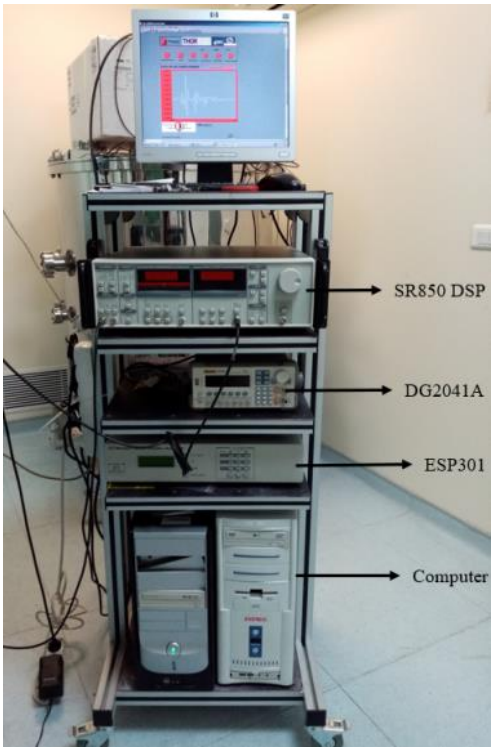

Figure 2.14 Data Acquisition

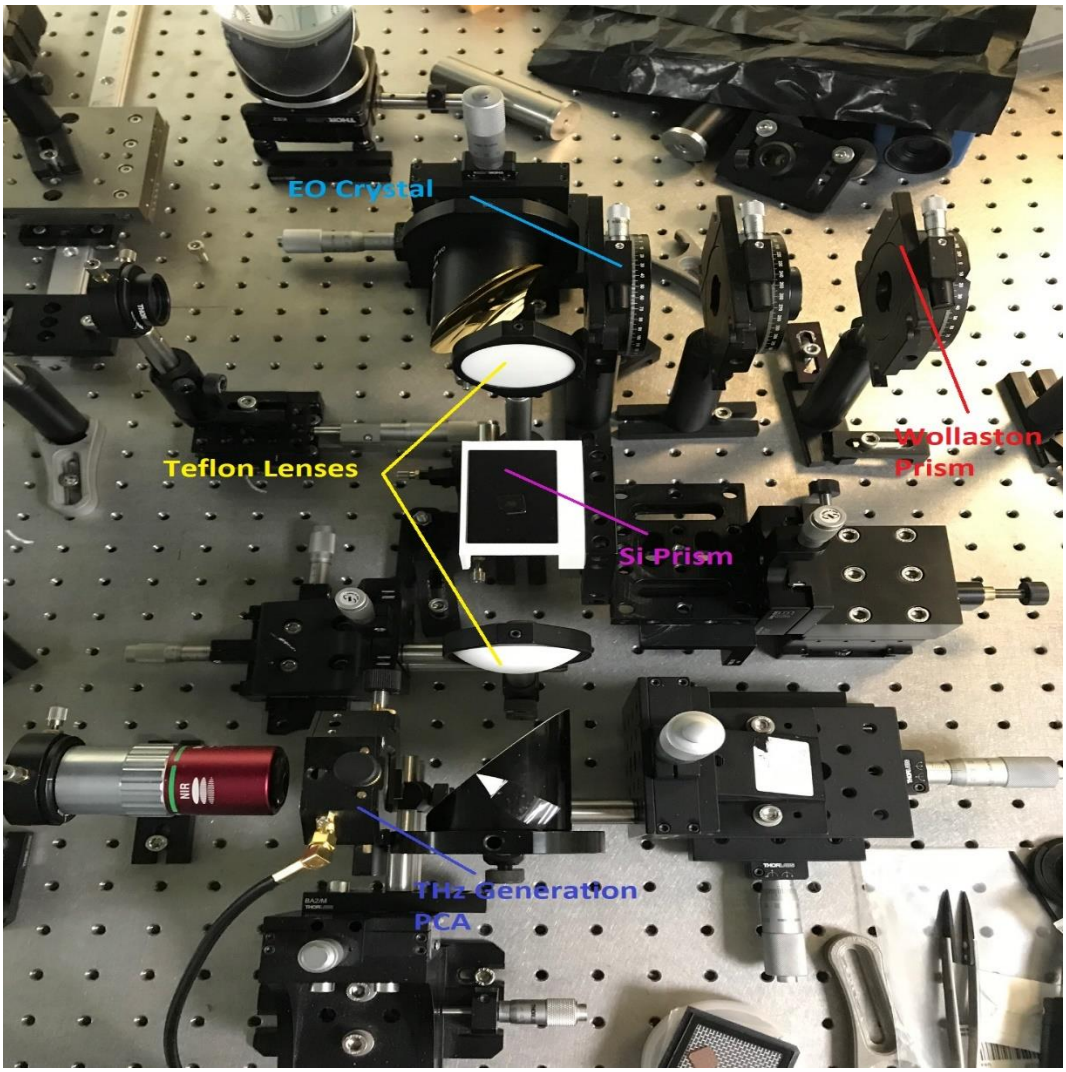

Figure 2.15 YDFL ATR System

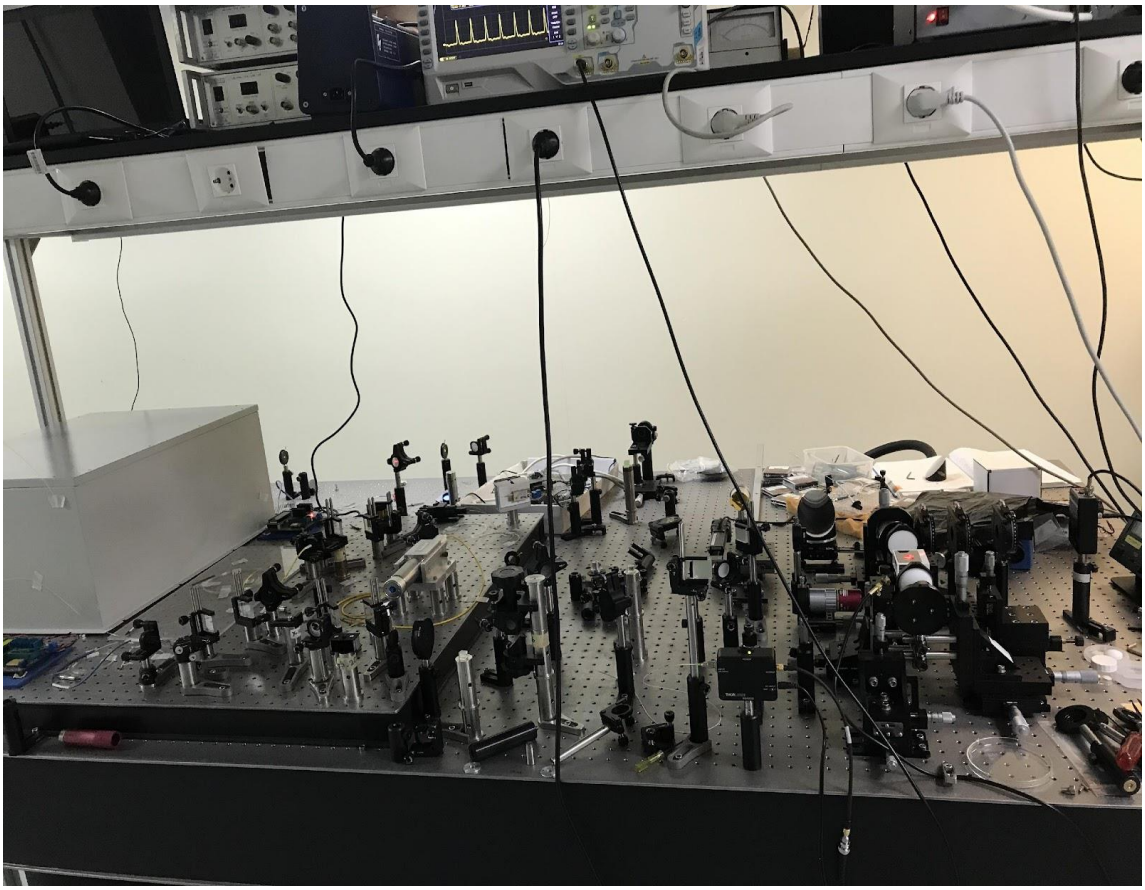

Figure 2.16 Whole YDFL THz ATR system on the optical table (left side is YDFL Laser system and right side is the ATR system)

The most important part of this system is the location of the ATR prism. The Si prism must be accurately aimed at with the incident THz beam. In order to achieve total internal reflection setup should be built carefully.

The THz beam's passage within and outside the ATR prism is simply demonstrated in figure below.

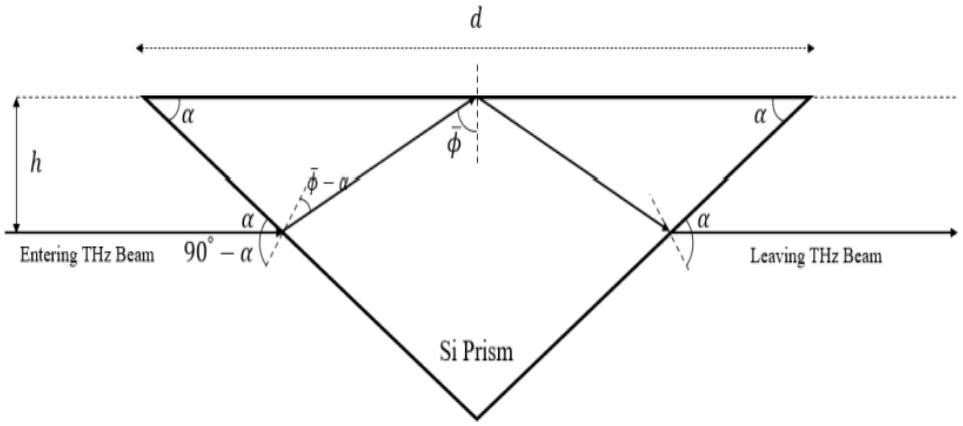

Figure 2.17 ATR Prism [8]

The incoming and exiting Terahertz beams are shown to be parallel to the prism's base.

Finding the angle $90 - \alpha$, which we shall refer to as β for simplicity, is the first step in calculating the angle $\overline{\emptyset}$.The system being constructed to deliver the incident Terahertz beam parallel to the prism base, and the angle α known from the prism's construction is established using the most basic geometrical principles. [8]

$$\alpha = 38.4° \tag{2.1}$$

$$\beta = 90° - 38.4° = 51.6° \tag{2.2}$$

To calculate $\overline{\emptyset} - \alpha$, Snell's Law can be used considering that the refractive index of the air is $n_{air} = 1$ and the refractive index of the prism is $n_{prism} = 3.42$.

$$n_{air} \sin\theta = n_{prism} \sin(\overline{\emptyset} - \alpha) \tag{2.3}$$

$$\sin 51.6 = 3.42 \sin(\overline{\emptyset} - \alpha) \tag{2.4}$$

$$(\overline{\emptyset} - \alpha) = \sin^{-1}\left(\frac{\sin 51.6}{3.42}\right) \tag{2.5}$$

$$(\overline{\emptyset} - \alpha) = 13.2° \tag{2.6}$$

$$\overline{\emptyset} = 13.2° + \alpha \tag{2.7}$$

$$\overline{\emptyset} = 13.2° + 38.4° = 51.6° \tag{2.8}$$

In order to obtain total internal reflection, the condition $\overline{\emptyset} > \overline{\emptyset_C}$ should be satisfied.

$$\overline{\emptyset_C} = \sin^{-1}\left(\frac{n_{sample}}{n_{prism}}\right) \tag{2.9}$$

$$\overline{\emptyset} > \overline{\emptyset_C} = \sin^{-1}\left(\frac{n_{sample}}{3.42}\right) \tag{2.10}$$

Equation 2.10 emphasize that there is a limit for the refractive index of the sample that this THz-ATR system can measure. Mathematically arranging the equation 2.10 can give this limit as shown in the below equation.

$$1 \leq n_{sample} \leq 2.68 \tag{2.11}$$

CHAPTER 3

ATR TERAHERTZ TIME DOMAIN SPECTROSCOPY

The optical properties of a wide range of materials, from liquids to semiconductors, have been determined using THz-TDS devices. [20] [21] [22]

However, due to their high absorbance at terahertz frequencies, measuring polar liquids, particularly water, has always been difficult. Considering the large volume of water included in biological materials, the inability to fully analyse water has restricted biological studies in the THz zone. In order to overcome this obstacle, various approaches, particularly those based on reflection spectroscopy, have been studied [36]. Hirori and others presented a novel approach termed attenuated total reflection (ATR) spectroscopy in 2004. [23]

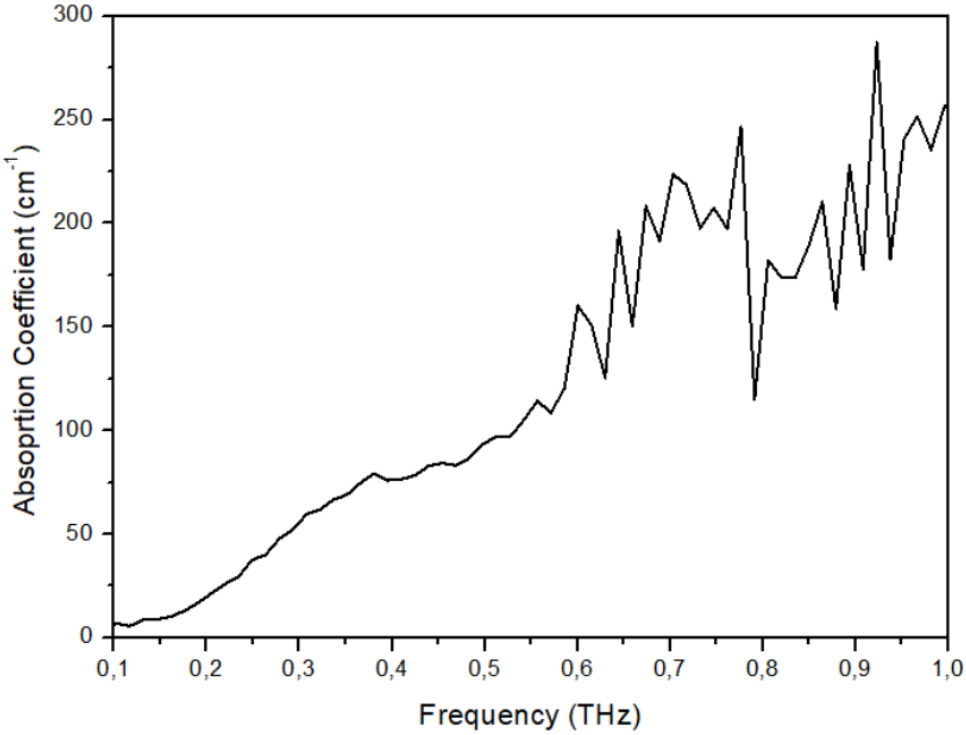

Figure 3.1 Plot for absorption coefficient of water between 0.1 to 1.0 THz

As it can be seen from the absorption coefficient graph of water, at 1.0 THz absorption coefficient is around 250 cm^{-1}.

Percentage of Terahertz signal loss can be calculated using the below formula. [24] "I" represent the intensity of the outcoming beam, "I_0" represents the incoming beam, "α" represents the absorption coefficient and "μ" represents the thickness of the sample.

$$I = I_0 e^{-\alpha\mu}$$

α is equal to 250 cm^{-1} at 1 THz and μ is equal to the 0.01 cm (100 micron). Adding the values to the formula gives $I = I_0 0.08$.

The loss can be calculated by

$$I_0 - I = I_0 - 0.08I_0 = 0.92I_0$$

By this simple calculation it can be seen that due to the high-water absorbance of THz, for 100-micron water sample at 1 THz signal loss is up to 92 percent.

3.1 Theory Behind ATR

In order to constructs a THz ATR-TDS system, total internal reflection, polarization of waves and penetration depth should be well understood considering that these are the most underlined parts of the theory behind ATR.

As indicated in the section 2.2 there are few important aspects that differs THz ATR-TDS system from THz-TDS system such as system geometry, ATR crystal etc. In order to constructs a THz ATR-TDS system, total internal reflection, polarization of waves and penetration depth should be well understood considering that these are the most underlined parts of the theory behind ATR.[34]

Inside the following chapters these concepts are explained.

3.1.1 Polarization

A simplified illustration of a critical part of a THz ATR-TDS system is shown below where the complete internal reflection and sample-THz interaction take place. The incident THz pulse from the emitter is focussed on the prism and reflected at the base of it by the total internal reflection (TIR). [25]

The figure below depicts a light beam propagating through a medium having refractive index n_1 and moving towards a medium having refractive index n_2. [8]

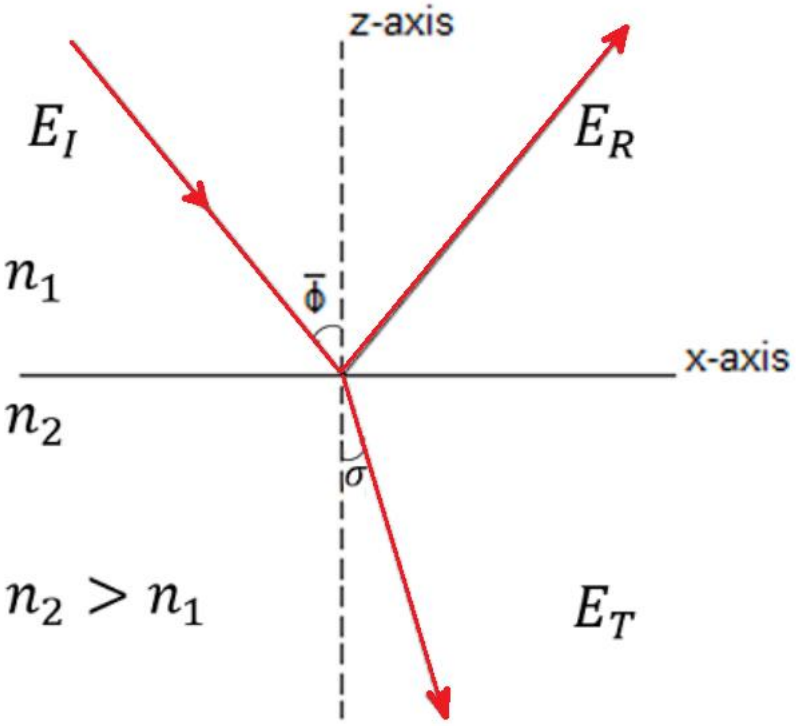

Figure 3.2 transmission and reflection between two media

As seen in the figure, E_R and E_T are the reflected and the transmitted parts respectively of the incident light E_I.

Inside a linear homogeneous medium, the equations of Maxwell can be seen in below equations.

$$\nabla \cdot E = 0 \tag{3.1}$$

$$\nabla \cdot B = 0 \tag{3.2}$$

$$\nabla \times E = -\frac{\partial B}{\partial t} \tag{3.3}$$

$$\nabla \times \mathrm{B} = \varepsilon\mu \frac{\partial E}{\partial t} \tag{3.4}$$

Below equations are the wave equations in three dimensions.

$$\nabla^2 E = \mu\varepsilon \frac{\partial^2 B}{\partial t^2} \tag{3.5}$$

$$\nabla^2 B = \mu\varepsilon \frac{\partial^2 E}{\partial t^2} \tag{3.6}$$

Wave functions for E and B are the equations 3.7 and 3.8 and they are the solutions to the above equations.

$$E(r,t) = E_0 e^{i(k\cdot r - \omega t)} \tag{3.7}$$

$$B(r,t) = B_0 e^{i(k\cdot r - \omega t)} \tag{3.8}$$

Maxwell's equations constraint equations by simply indicating that the wave functions should have a perpendicularity as in equation 3.9. Thus, considering this equations 3.7 and 3.8 can have a form as 3.10 and 3.11.

$$B(r,t) = \frac{1}{v} E_0 \hat{k} \times \hat{E} \tag{3.9}$$

$$E(r,t) = E_0 e^{i(k\cdot r - \omega t)} \hat{n} \tag{3.10}$$

$$B(r,t) = \frac{1}{v} E_0 e^{i(k\cdot r - \omega t)} (\hat{k} \times \hat{n}) \tag{3.11}$$

$$v = \frac{1}{\sqrt{\varepsilon\mu}} = \frac{c}{n} \tag{3.12}$$

$$n \equiv \sqrt{\frac{\varepsilon\mu}{\varepsilon_0 \mu_0}} \tag{3.13}$$

Below are the boundary conditions.

$$\varepsilon_1 E_1^{\perp} = \varepsilon_2 E_2^{\perp} \tag{3.14}$$

$$B_1^{\perp} = B_2^{\perp} \tag{3.15}$$

$$E_1^{\parallel} = E_2^{\parallel} \tag{3.16}$$

$$\frac{1}{\mu_1} B_1^{\parallel} = \frac{1}{\mu_2} B_2^{\parallel} \tag{3.17}$$

The tangential components of the electric field are continuous at a boundary, whereas the normal components have a jump based on the dielectric constants of the two mediums. [26][34]

The tangential components of the magnetic field, have a jump that is dependent on the magnetic permeability of the media, but the normal components are continuous and the assumption of $\mu \cong \mu_0$ for the two media is reduced to $n \cong \sqrt{\varepsilon_r}$. [26] [27][35]

Rearranged boundary conditions for incident, transmitted and reflected wave can be seen in below equations.

$$\varepsilon_1(\boldsymbol{E}_I^{\perp} + \boldsymbol{E}_R^{\perp}) = \varepsilon_2 E_T^{\perp} \tag{3.18}$$

$$n_1 \boldsymbol{k}_I \times \boldsymbol{E}_I^{\perp} + n_1 \boldsymbol{k}_R \times \boldsymbol{E}_R^{\perp} = n_2 \boldsymbol{k}_T \times \boldsymbol{E}_T^{\perp} \tag{3.19}$$

$$(\boldsymbol{E}_I^{\parallel} + \boldsymbol{E}_R^{\parallel}) = \boldsymbol{E}_T^{\parallel} \tag{3.20}$$

$$n_1 \boldsymbol{k}_I \times \boldsymbol{E}_I^{\parallel} + n_1 \boldsymbol{k}_R \times \boldsymbol{E}_R^{\parallel} = n_2 \boldsymbol{k}_T \times \boldsymbol{E}_T^{\parallel} \tag{3.21}$$

Further calculations are heavily influenced by the incident wave's polarization. As a result, it's advisable to look at both s- and p-polarized waves individually. Below equations are identity and Snell's law. [8]

$$(E_I + E_R) = E_T \tag{3.22}$$

$$n_1(E_I - E_R)\cos\overline{\emptyset} = n_2 E_T \cos\sigma \tag{3.23}$$

Noting that the $r^s \; and \; t^s$ are the reflection coefficient and the transmission coefficient, equations 3.22 and 3.23 can take the below forms.

$$r^s = \frac{E_R}{E_I} = \frac{n_1 \cos\overline{\emptyset} - \sqrt{n_2^2 - n_1^2 \sin^2\overline{\emptyset}}}{n_1 \cos\overline{\emptyset} + \sqrt{n_2^2 - n_1^2 \sin^2\overline{\emptyset}}} \tag{3.24}$$

$$t^s = \frac{E_T}{E_I} = \frac{2n_1 \cos\overline{\emptyset}}{n_1 \cos\overline{\emptyset} + \sqrt{n_2^2 - n_1^2 \sin^2\overline{\emptyset}}} \tag{3.25}$$

Now same procedure is repeated in the below equations for the p-polarized waves noting that $r^p \; and \; t^p$ are the reflection coefficient and the transmission coefficient.

$$(E_I - E_R)\cos\overline{\emptyset} = E_T \cos\sigma \tag{3.26}$$

$$n_1(E_I + E_R) = n_2 E_T \tag{3.27}$$

$$r^p = \frac{E_R}{E_I} = \frac{n_2^2 \cos\overline{\emptyset} - n_1\sqrt{n_2^2 - n_1^2 \sin^2\overline{\emptyset}}}{n_2^2 \cos\overline{\emptyset} + \sqrt{n_2^2 - n_1^2 \sin^2\overline{\emptyset}}} \tag{3.28}$$

$$t^p = \frac{E_T}{E_I} = \frac{2n_1 n_2 \cos\overline{\emptyset}}{n_2^2 \cos\overline{\emptyset} + n_1\sqrt{n_2^2 - n_1^2 \sin^2\overline{\emptyset}}} \tag{3.29}$$

3.24, 3.25, 3.28 and 3.29 are known as the Fresnel coefficients. Equation 3.30 represents the Snell's law.

$$n_2 \sin\overline{\emptyset} = n_1 \sin\sigma \tag{3.30}$$

Below equations now show the Fresnel equations considering both s-polarized and p-polarized waves.

$$r^s = \frac{E_R}{E_I} = \frac{n_1 \cos\overline{\emptyset} - \sqrt{n_2^2 - n_1^2 \sin^2\overline{\emptyset}}}{n_1 \cos\overline{\emptyset} + \sqrt{n_2^2 - n_1^2 \sin^2\overline{\emptyset}}} \tag{3.31}$$

$$r^p = \frac{E_R}{E_I} = \frac{n_2^2 \cos\overline{\emptyset} - n_1\sqrt{n_2^2 - n_1^2 \sin^2\overline{\emptyset}}}{n_2^2 \cos\overline{\emptyset} + \sqrt{n_2^2 - n_1^2 \sin^2\overline{\emptyset}}} \tag{3.32}$$

The s type polarization occurs when the electric field is perpendicular to the incidence plane. The p-type polarization occurs when the electric field is parallel to the incidence plane. For the THz beam, p type polarization being less affected due to secondary reflections and deflections of the prism is proven. Even if there is no strict constraint for choosing between s and p type polarization, considering this advantage of the p type polarization makes it more preferable for the THz systems. [28]

3.1.2 Theory of Penetration Depth

Inside the section 2.2 the evanescent wave resulting from total internal reflection used in the ATR spectroscopy system is explained. As evanescent wave propagates, an electromagnetic field penetrates the other side of the interface and decays exponentially. The evanescent wave's decay is expressed as 3.38 where α represents the decay constant which is mostly depend on the refractive index. [8][40]

$$e^{-r\alpha} \tag{3.38}$$

Below equations are the vector forms of the reflected and transmitted waves remembering the Figure 3.1 and considering that k is the wave number and k_0 is $\frac{w}{c}$ in vacuum and also $n_1$is less dense medium.[36]

$$\boldsymbol{E}_R(r,t) = E_R e^{i(k_t \cdot r - \omega t)} \tag{3.39}$$

$$\boldsymbol{E}_T(r,t) = E_T e^{i(k_r \cdot r - \omega t)} \tag{3.40}$$

$$\frac{\omega}{k_t} = \frac{c}{n_1} \tag{3.41}$$

$$k_t = \frac{n_1 \omega}{c} \tag{3.42}$$

$$k_t = n_1 k_0 \tag{3.43}$$

$$k_t = n_1 k_0 (z\cos\sigma + x\sin\sigma) \tag{3.44}$$

After applying the Snell's Law to 3.44 following equations can be obtained noting that σ is angle of refrection.

$$k_t = k_0 (z n_1 \cos\sigma + x n_2 \sin\overline{\emptyset}) \tag{3.45}$$

$$k_t \cdot r = k_0 (n_2 x \sin\overline{\emptyset} + n_1 z\cos\sigma \tag{3.46}$$

$$\boldsymbol{E}_T(\boldsymbol{r}, t) = \boldsymbol{E}_T e^{i(n_2 k_0 x \sin\overline{\emptyset} + n_1 k_0 z\cos\sigma - \omega t)} \tag{3.47}$$

Writing σ in terms of the $\overline{\emptyset}$ is very important because when total internal reflection occurs refraction angle should not exist.

$$\cos\sigma = \sqrt{1-\sin^2\sigma} = \sqrt{1-(n_2/n_1)^2\sin^2\overline{\emptyset}} \tag{3.48}$$

$$k_0(n_2 x\sin\overline{\emptyset} + n_1 z\cos\sigma) = k_0\left(n_2 x\sin\overline{\emptyset} + z n_1\sqrt{1-(n_2/n_1)^2\sin^2\overline{\emptyset}}\right) \tag{3.49}$$

$$\boldsymbol{E}_T(\boldsymbol{r}, t) = \boldsymbol{E}_T e^{-i\omega t} e^{i n_2 k_0 x\sin\overline{\emptyset}} e^{-k_0 z\sqrt{n_2^2\sin^2\overline{\emptyset} - n_1^2}} \tag{3.50}$$

Combining with the equation 3.50 following equations are obtained.

$$\boldsymbol{E}_T(r, t) = \boldsymbol{E}_T e^{-\alpha z} e^{-i(k\cdot x - \omega t)} \tag{3.51}$$

$$\alpha = k_0 z\sqrt{n_2^2\sin^2\overline{\emptyset} - n_1^2} \tag{3.52}$$

$$d_p = \frac{1}{k_0 z\sqrt{n_2^2\sin^2\overline{\emptyset} - n_1^2}} = \frac{c}{2\pi v_0\sqrt{n_2^2\sin^2\overline{\emptyset} - n_1^2}} \tag{3.53}$$

Where d_p represents the penetration depth. The investigation of the penetration depth equation gives that the first exponential section of the formula is actually the wave's oscillatory nature, second is the wave propagation along x-axis in the figure 3.2 and finally third section is the evanescent wave's exponential decay.

Plotting the penetration depth values according to the equation 3.53, possible measurement intervals can be defined for the built THz-ATR system as shown in the figure below.

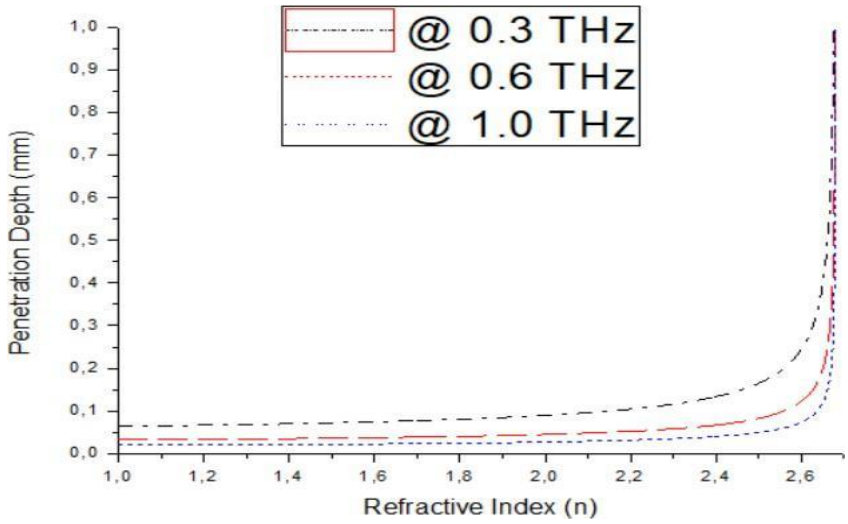

Figure 3.3 Penetration Depth Plot at Different THz Frequencies

Plot shown in figure 3.3 shows that the samples which have refractive index around 1.4 measured between 0.3 to 1.0 THz have penetration depth up to 0.1 mm.

3.2 Formulation of Complex Refractive Index of Samples Measured with THz ATR Spectroscopy

The system's reference and sample signals are compared mathematically in time domain analysis. [15] For the analyse reference signal and sample signal are expressed respectively as $E_{ref}(t)$ and $E_{sample}(t)$.

These signals should be transformed into the frequency domain for better analysis and to do so Fourier transform is used.

$$E_{ref}(t) \overset{FT}{\rightarrow} = \frac{1}{\sqrt{2\pi}} \int_{-\infty}^{\infty} E_{ref}(t) e^{-i\omega t}\, dt = E_{ref}(\omega) \tag{3.54}$$

$$E_{sample}(t) \overset{FT}{\rightarrow} = \frac{1}{\sqrt{2\pi}} \int_{-\infty}^{\infty} E_{sample}(t) e^{-i\omega t}\, dt = E_{sample}(\omega) \tag{3.55}$$

Signal ratio is the same with Fresnel coefficient's ratio.

$$\frac{E_{sample}(\omega)}{E_{ref}(\omega)} = \frac{r_{sample}}{r_{ref}} \tag{3.56}$$

As explained in the section 3.1.1 preferring the p-type polarization is advantageous.[37] Because of that the below equations took the form in accordance to the p-type polarization noting that the R states for amplitude and κ states for the phase

$$\frac{E_{sample}(\omega)}{E_{ref}(\omega)} = Re^{(i\kappa)} = \frac{r^{p}_{sample}}{r^{p}_{ref}} \tag{3.57}$$

$$r^{p}_{sample} = r^{p}_{ref} Re^{(i\kappa)} \tag{3.58}$$

The n_1 and n_2 inside Equation 3.32 which is the equation for the p-polarized Fresnel coefficient are represents the refractive index for the sample and the prism respectively. In below, equation 3.32 is rewritten accordingly.

$$r_{sample}^{p} = \frac{n_{sample}^{2}\cos\overline{\emptyset} - n_{prism}\sqrt{n_{sample}^{2} - n_{prism}^{2}\sin^{2}\overline{\emptyset}}}{n_{sample}^{2}\cos\overline{\emptyset} + n_{prism}\sqrt{n_{sample}^{2} - n_{prism}^{2}\sin^{2}\overline{\emptyset}}} \tag{3.59}$$

In order to provide convenience for the further calculations, equation 3.60 is used where $(r_{sample}^{p} - 1)^2 = Y \; and \; (r_{sample}^{p} + 1)^2 = X$

$$n_{sample}^{2} = \epsilon_{sample} = \frac{X \pm \sqrt{X^2 - YX\sin^2 2\overline{\emptyset}}}{2Y\cos^2\overline{\emptyset}} \tag{3.60}$$

$$n_{sample} = n'_{sample} + ik_{sample} \tag{3.61}$$

$$n_{sample}^{2} = \epsilon_{sample} = \epsilon'_{sample} + i\epsilon''_{sample} \tag{3.62}$$

$$\epsilon'_{sample} = n'^{2}_{sample} - k_{sample}^{2} \tag{3.63}$$

$$\epsilon''_{sample} = 2n'_{sample}k_{sample} \tag{3.64}$$

Since all materials have $\epsilon'' > 0$ positive solutions should be taken. [29]. So the complex refractive index can be written as in the forms of equations 3.63 and 3.64.

CHAPTER 4

ATR TERAHERTZ TIME DOMAIN SPECTROSCOPY MEASUREMENTS AND DATA ANALYSIS

4.1 Data Acquisition

The program that executes data acquisition in the system was previously written in Labview.

In order to record the value of the Terahertz signal obtained from the lock-in amplifier output at each translational stage step, which corresponds to a predetermined time interval, and to construct the entire waveform in time domain, the software provides communication between the translational stage controller and the lock-in amplifier. [8]

Python and Origin Pro 8 are both used to analyse the captured THz data. Also, both Origin Pro 8 and Python are used to perform FFT calculations on the data that has been processed.

4.2 Biological Samples

In this thesis biological samples are analysed which are soft tissues that have different type of lesions taken from the Faculty of Dentistry of Ankara University with the ethical approval.

The first and second tissue samples are peripheral giant cell granuloma. The third tissue sample is Pleomorphic adenoma. The fourth and fifth tissue samples are Fibrosis polyp.

The refractive index of mammalian soft tissues is measured with different methods and found to be approximately the same values as $1.3818 \pm 0.0049i$. [30]

For the further biological sample analysis, the refractive index of the biological samples is assumed to be 1.38 as explained above in order to test the performance of our system by comparing the expected sample signal based on the assumed refractive index of biological samples with the measured signal of our Terahertz ATR Spectroscopy system.

During measurements, tissue samples were located directly on the Silicon prism.

Each sample was placed without harming the samples to ensure that they were completely in touch with the surface of the prism.

According to the Figure 3.3 at 0.3 THz, 1.38 sample refractive index has penetration depth close to 0.1 mm.

Below figures show the 5 different mouth tissue samples and the marker laser spot is what's causing the vivid red blazing.

Figure 4.1Tissue Sample 1 on ATR Prism Surface

4.2 Tissue Sample 2 on ATR Prism Surface

Figure 4.3 Tissue Sample 3 on ATR Prism Surface

Figure 4.4 Tissue Sample 4 on ATR Prism Surface

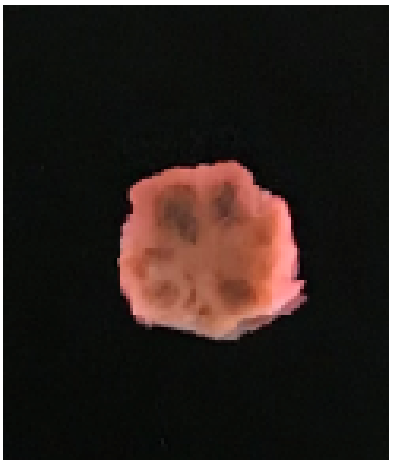

Figure 4.5 Tissue Sample 5 on ATR Prism Surface

4.3 Inverse Fourier Analysis and Results

This section will discuss the principles that underlie sample measurements as well as the analysis of time domain data that has been acquired.

Mathematically comparing the system's obtained sample and reference signals is the basis of the time domain analysis. [15][39][44]

A reference signal is recorded with a THz ATR-TDS system with nothing on the base of Silicon prism. While samples are measured by positioning them where the THz beam is concentrated and reflected. A crucial aspect of measurements is the sample's alignment to the Terahertz focal point.

An expression for a reference measurement in the time domain is $E_{ref}(t)$.Likewise, $E_{sample}(t)$ becomes the expression for sample measurements (t). This also means that the expression for the reference measurement in frequency domain is $E_{ref}(\omega)$ and the expression for the sample measurement in frequency domain is $E_{sample}(\omega)$.

Since the aim of the analysis is to be able to have an idea about the system performance, acquired sample signal should be compared to the expected sample signal. Following equation arrangements are made in order to discover the expected sample signal.

Rearranging the equation 3.57 which is derived in previous sections, expected sample signal can be acquired by knowing the refractive index of the sample which is shown as equation 3.58.

$$\frac{E_{sample}(\omega)}{E_{ref}(\omega)} = \frac{r_{sample}^{p}}{r_{ref}^{p}} \tag{3.57}$$

$$E_{sample}(\omega) = E_{ref}(\omega)\frac{r_{sample}^{p}}{r_{ref}^{p}} \tag{3.58}$$

Acquired reference signal from the setup is in the time domain however as the equation 3.57 indicates signal should be in frequency domain. Because of this first

the reference signal should be transferred into frequency domain by Fourier Transform as in the below.

$$E_{ref}(t) \overset{FT}{\rightarrow}= \frac{1}{\sqrt{2\pi}} \int_{-\infty}^{\infty} E_{ref}(t) e^{-i\omega t}\, dt = E_{ref}(\omega) \tag{3.65}$$

Then equation 3.57 is applied and the expected sample signal is acquired in the frequency domain. Again, however our measured sample signal is acquired from the setup in time domain. In order to compare the expected sample signal and the measured sample signal, Inverse Fourier Transformation must be applied to transfer the signal back into the time domain as below.

$$E_{sample}(\omega) \overset{IFT}{\longrightarrow}= \int_{-\infty}^{\infty} E_{sample}(\omega) e^{i\omega t}\, d\omega = E_{refsample}(t) \tag{3.66}$$

Measurements in time-domain with Terahertz Time Domain ATR Spectroscopy system for the biological tissues are given in below as Figure 4.6, Figure 4.7, Figure 4.8, Figure 4.9, Figure 4.10.

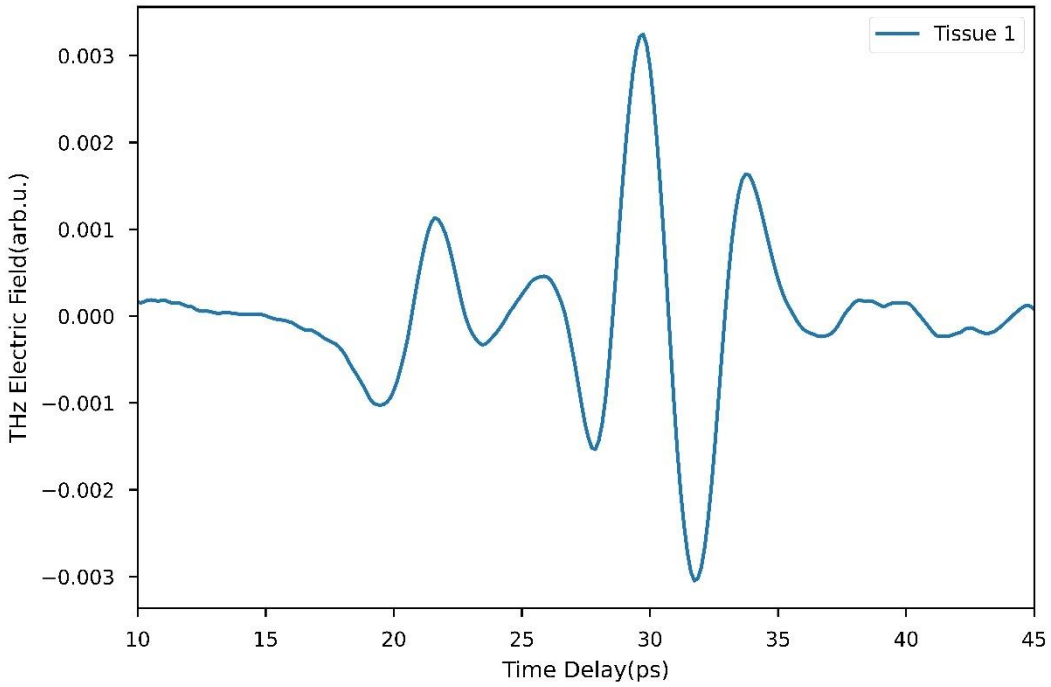

Figure 4.6 Time Domain Measurement for the Tissue Sample 1

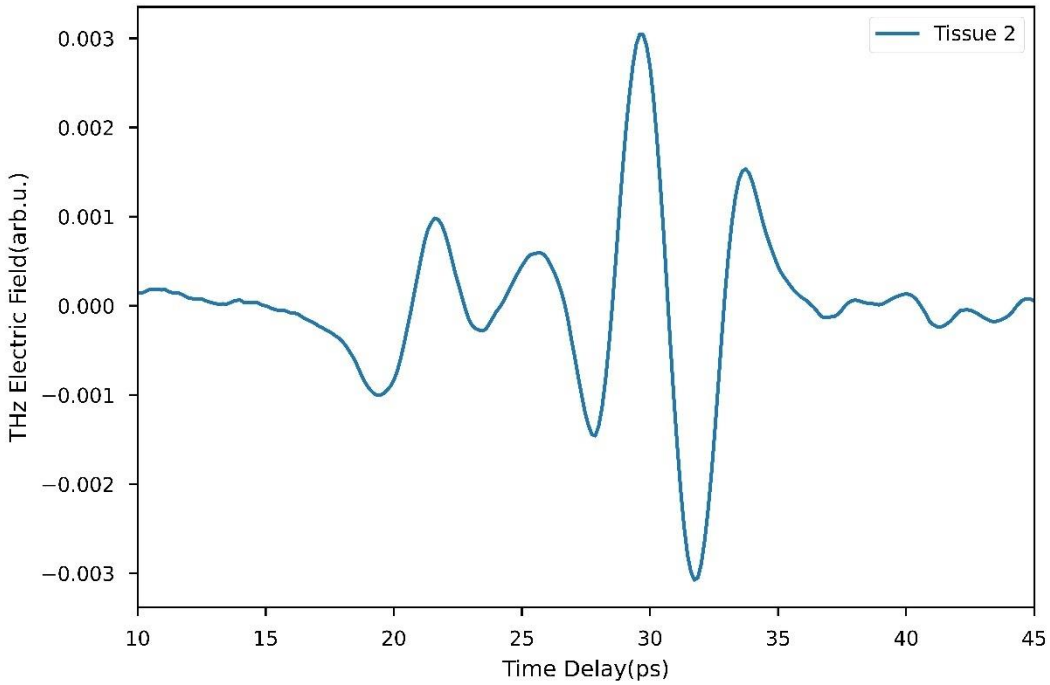

Figure 4.7 Time Domain Measurement for the Tissue Sample 2

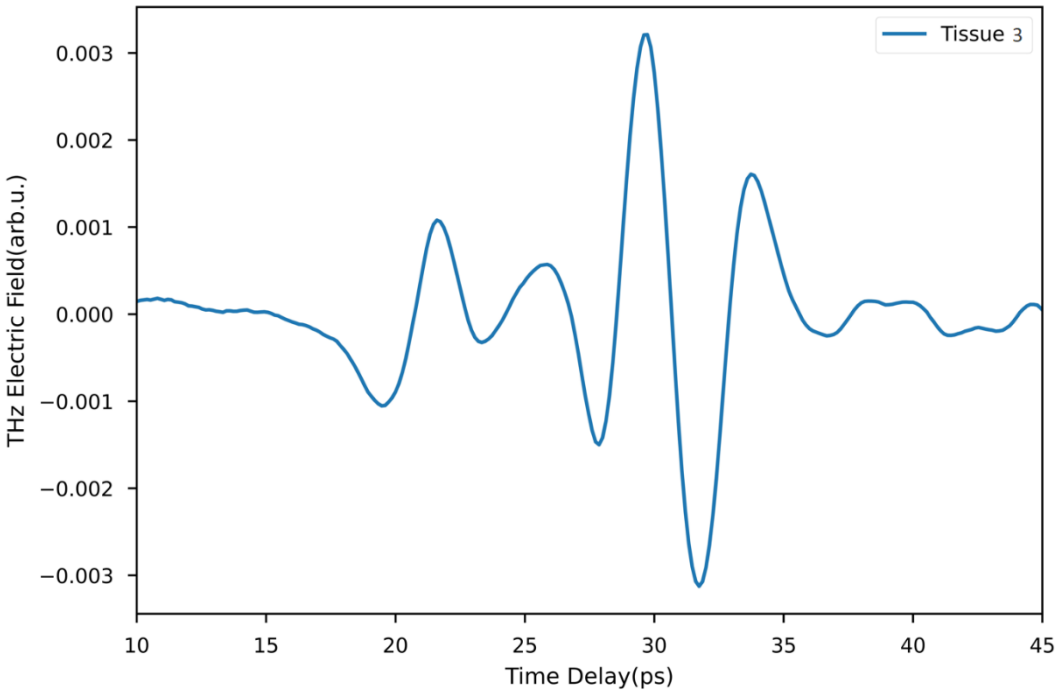

Figure 4.8 Time Domain Measurement for the Tissue Sample 3

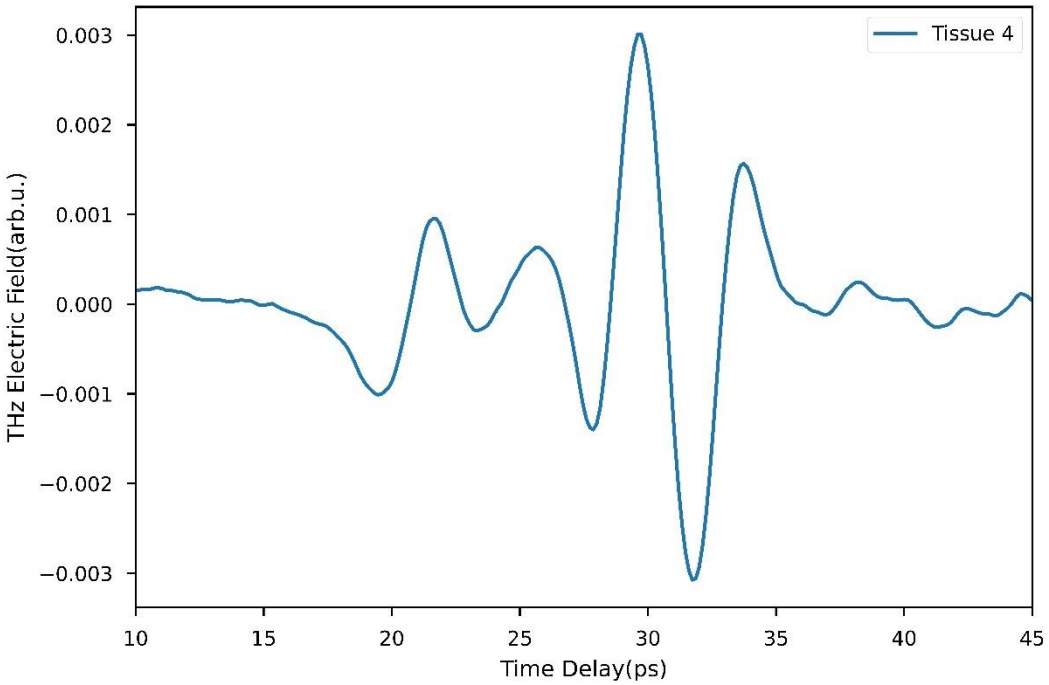

Figure 4.9 Time Domain Measurement for the Tissue Sample 4

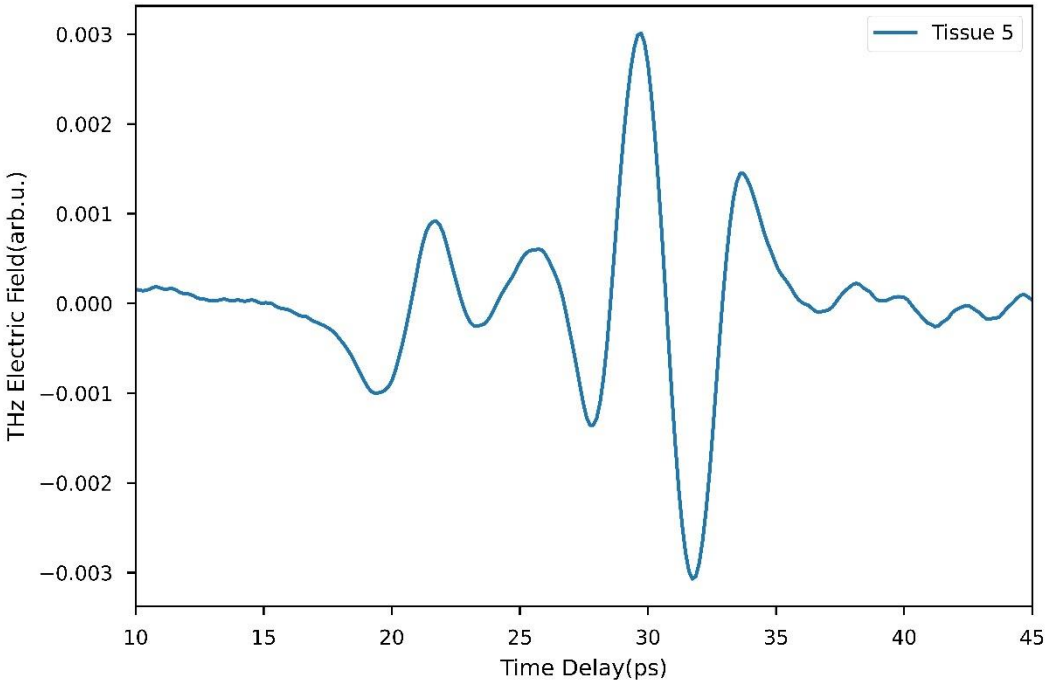

Figure 4.10 Time Domain Measurement for the Tissue Sample 5

In the below Figure 4.11 shows the THz-ATR Time Domain measurements of the biological tissues and the reference signal together.

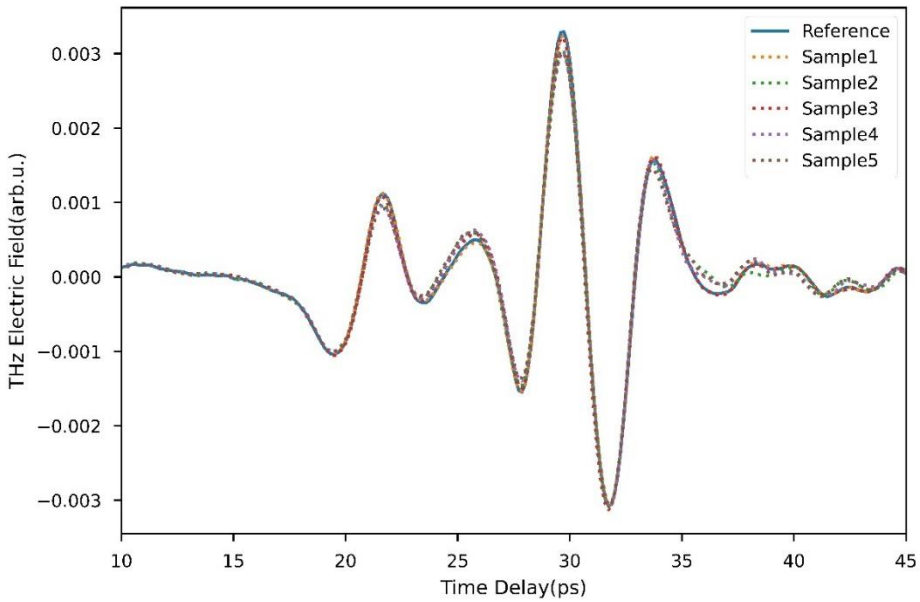

Figure 4.11 Time Domain Measurement for the all-Tissue Samples and Reference Measurement

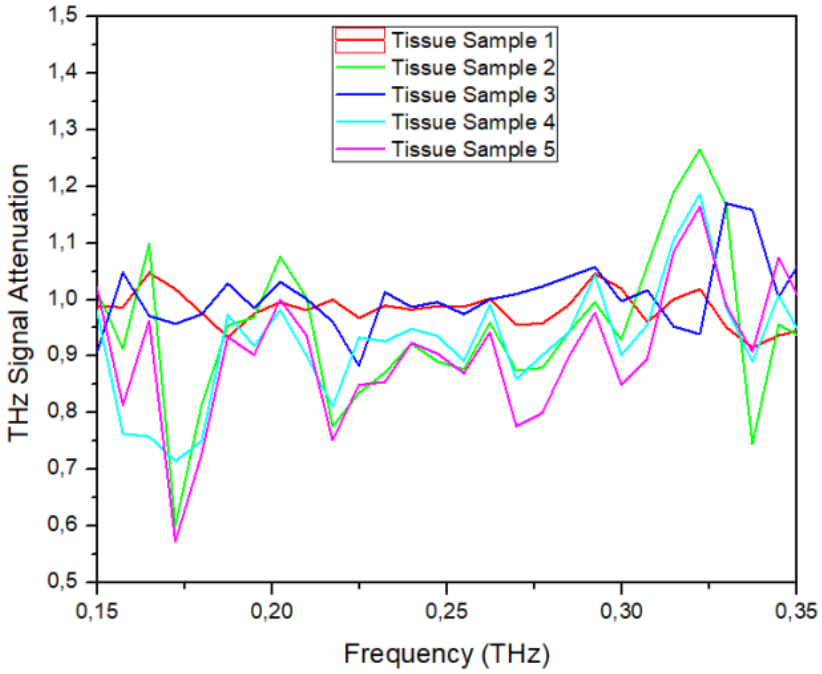

Figure 4.12 Signal Attenuation up to 1 THz

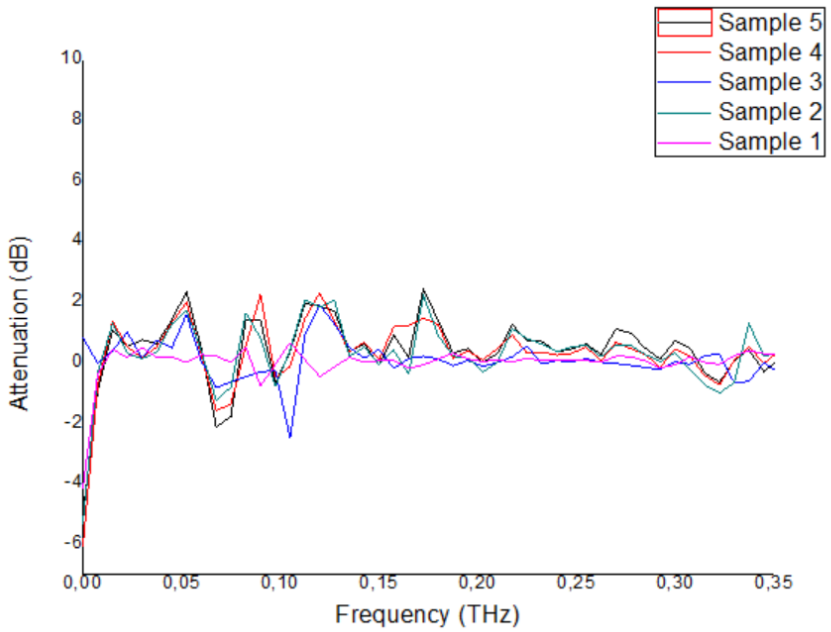

Figure 4.13 Signal Attenuation in dB in the frequency range 0.15- 0.35 THz

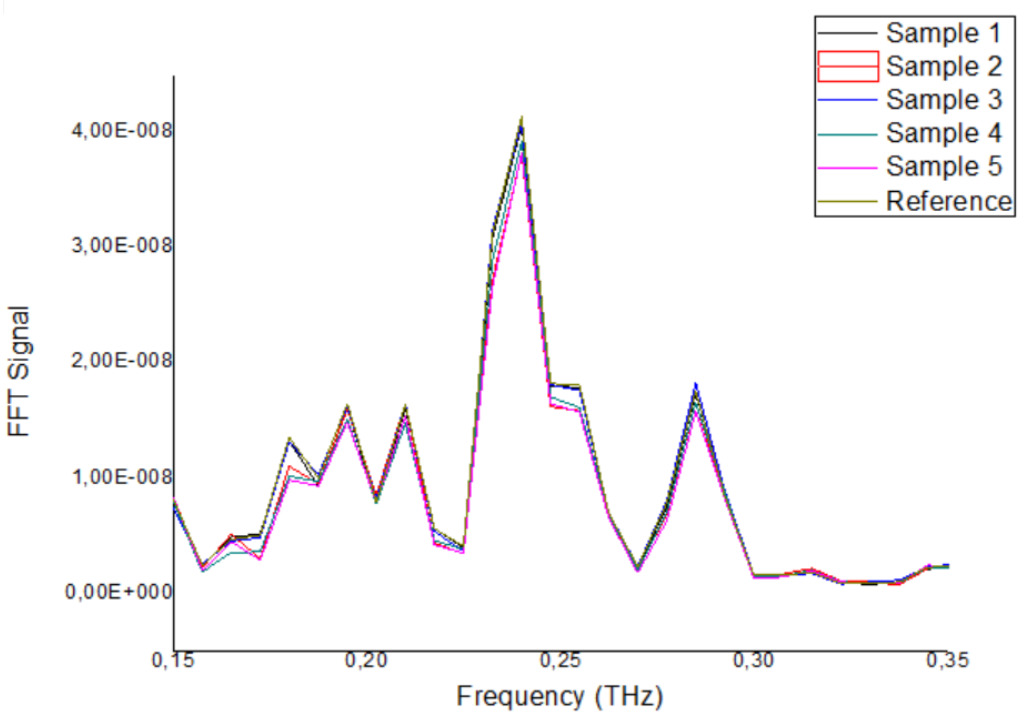

Figure 4.14 Experimental Sample Signals in Frequency Domain

Figure 4.12 and Figure 4.13 shows that the frequency interval for the system is in between 0.15 and 0.35 THz.

After applying the inverse Fourier analysis, expected sample signals and obtained sample signals are compared and shown in the below figures which are Figure 4.15, Figure 4.16Figure 4.15, Figure 4.17, Figure 4.18 and Figure 4.19. In the figures, “sample” represents the expected sample signal that is calculated. “Tissue 1”, “Tissue 2”, “Tissue 3”, “Tissue 4”, “Tissue 5” represent the obtained sample signals for the tissue 1, tissue 2, tissue 3, tissue 4 and the tissue 5 respectably.

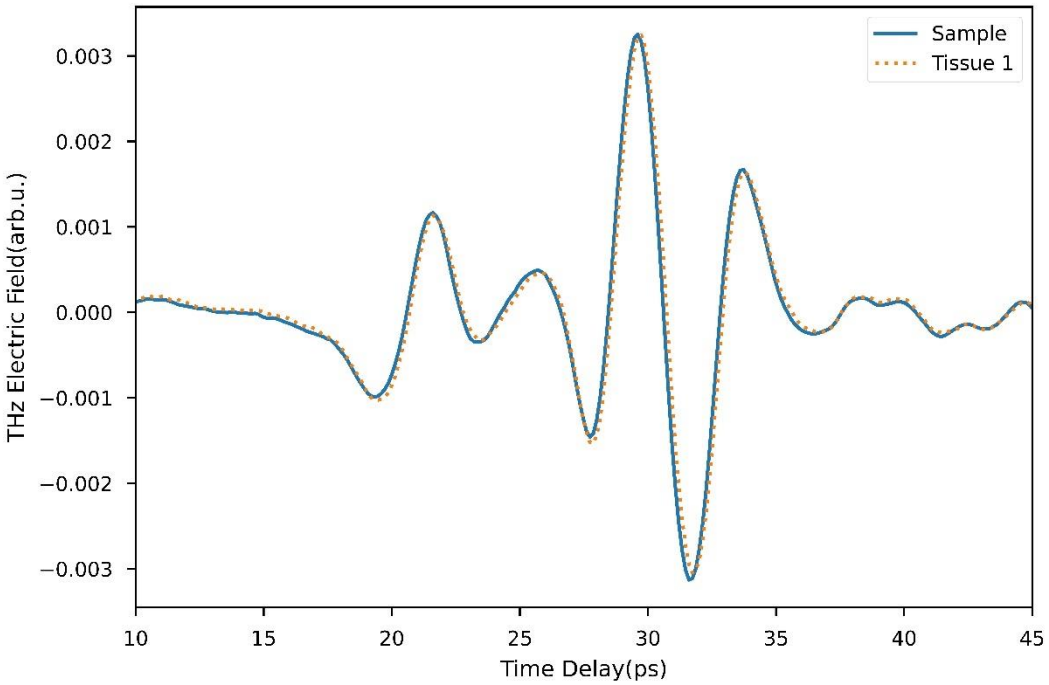

Figure 4.15 Comparison of IFFT Analysis for the Tissue Sample 1 and Time Domain measurement for the Tissue Sample 1

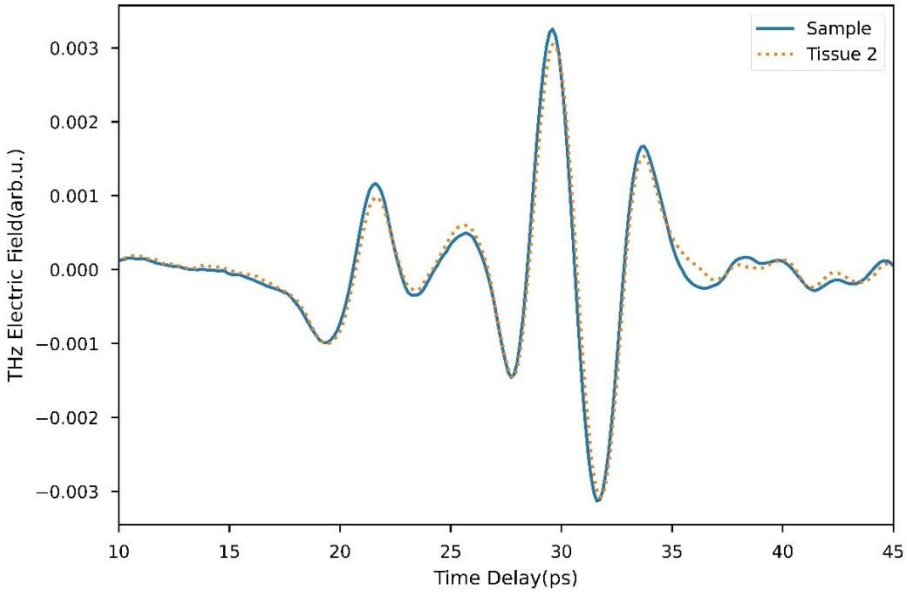

Figure 4.16 Comparison of IFFT Analysis for the Tissue Sample 2 and Time Domain measurement for the Tissue Sample 2

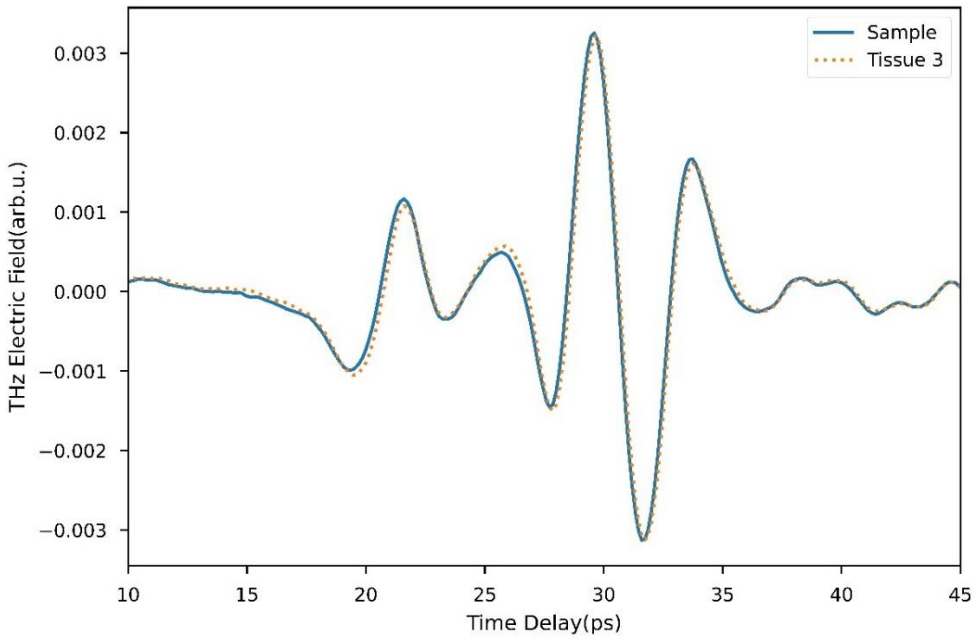

Figure 4.17 Comparison of IFFT Analysis for the Tissue Sample 3 and Time Domain measurement for the Tissue Sample 3

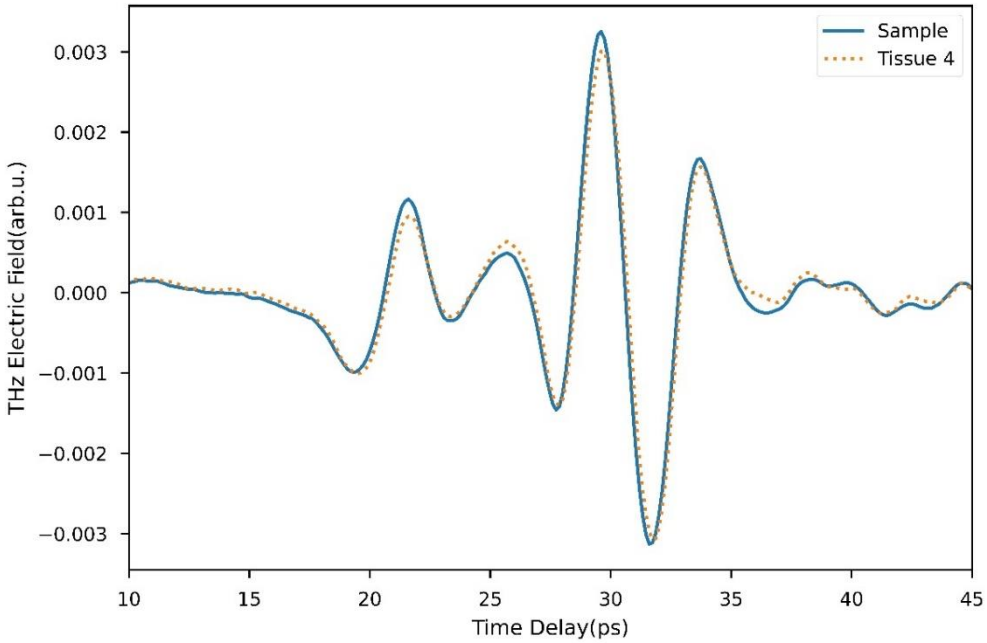

Figure 4.18 Comparison of IFFT Analysis for the Tissue Sample 4 and Time Domain measurement for the Tissue Sample 4

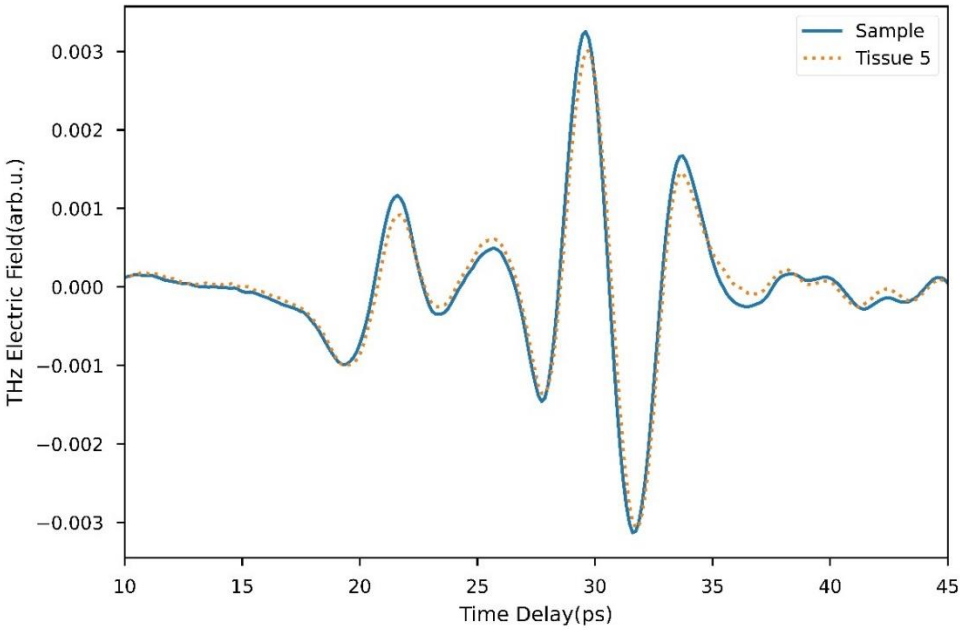

Figure 4.19 Comparison of IFFT Analysis for the Tissue Sample 5 and Time Domain measurement for the Tissue Sample 5

In the below, Figure 4.20 and Figure 4.21 shows the comparison for the obtained sample signal and expected sample signal for all the tissue samples together.

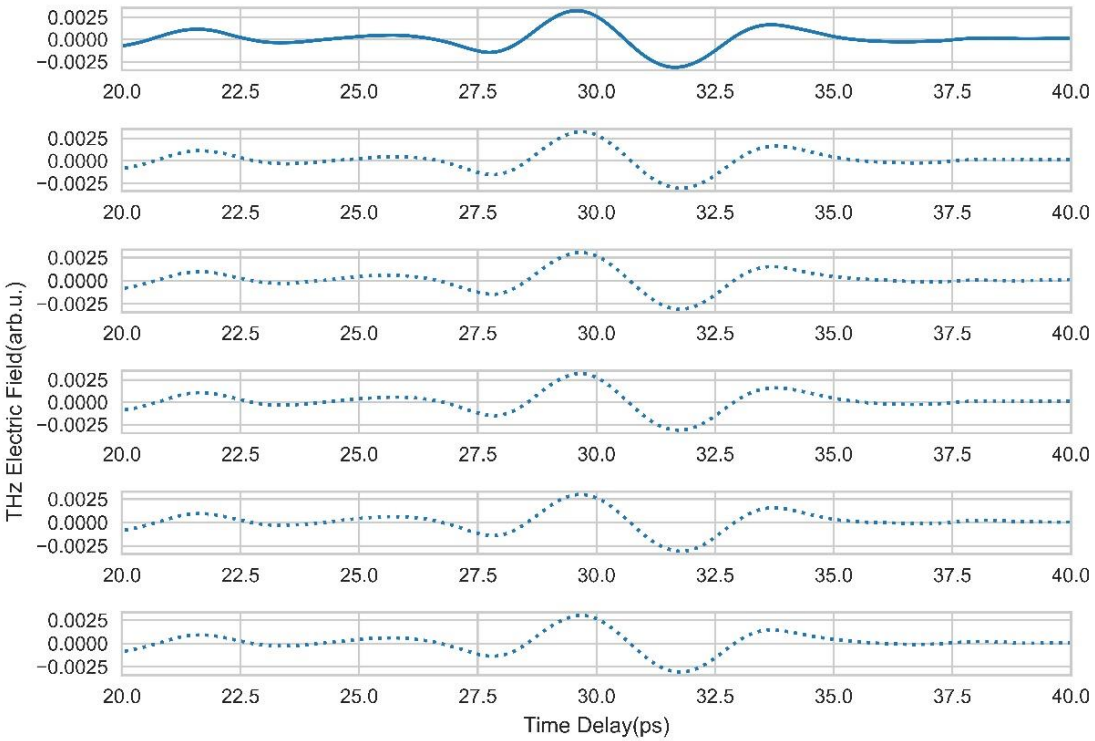

Figure 4.20 Comparison of IFFT Analysis for all Tissue Samples and Time Domain measurements zoomed.

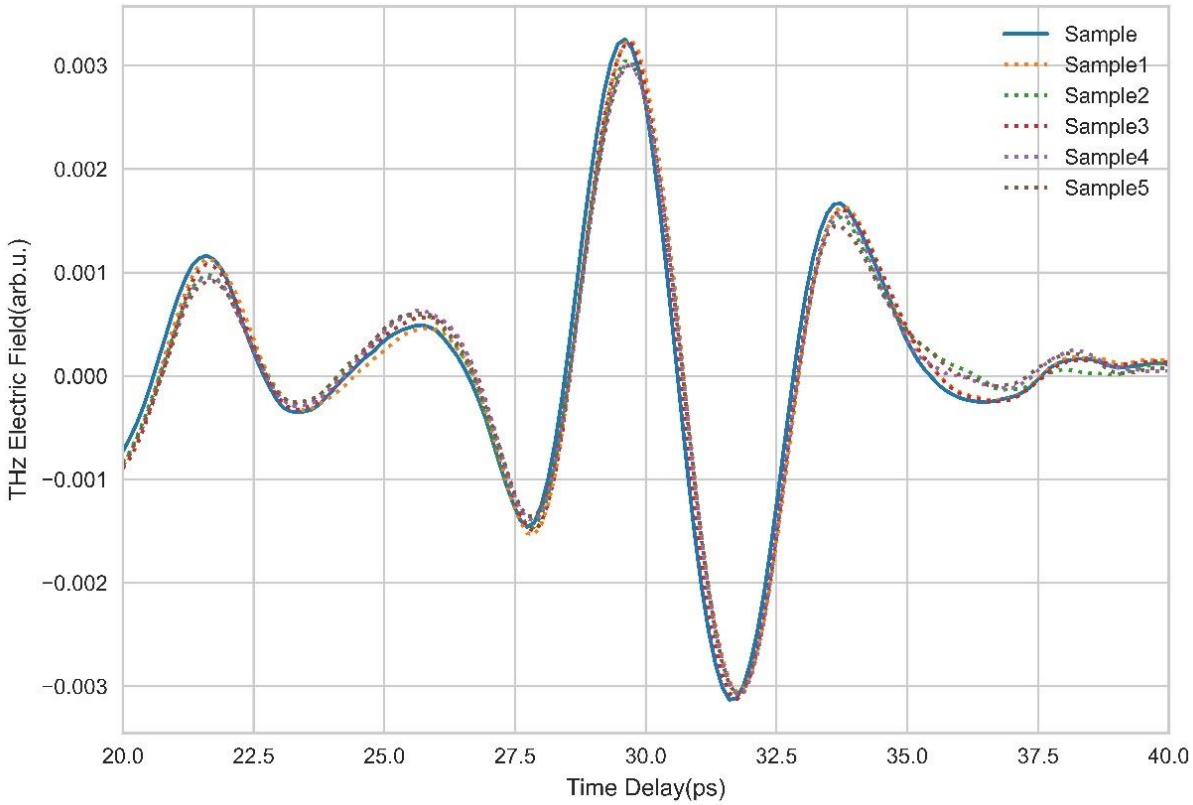

Figure 4.21 Comparison of IFFT Analysis for all Tissue Samples and Time Domain measurements together.

4.4 DISCUSSION

As indicated in the section 2.2.1, YDFL THz-ATR time domain system used in this thesis has a narrow bandwidth. Despite this drawback, the results depicted in Figures 4.6-4.10 demonstrate that water absorption did not cause the THz signal to be lost during the experiments. If Figure 4.11 is analysed, it can be seen that time scale differences and the signal level differences can be easily detected.These can indicate the refractive index differences between the tissues due to different infections or the different amount of infections for the same infections.

In order to simulate the expected sample signals one refractive index value is chosen and used for all 5 tissues accordingly to the previous studies considering that all of them shows approximately same value even for the different types of biological tissues due to the high amount of water contained in the biological samples.

If the figures 4.15-4.19 are analysed it can be seen that the simulated sample signals are highly close to the experimentally measured sample signals. Small difference between them represents small refractive index difference between the chosen biological soft tissue refractive index from the previous studies and the unknown refractive index of the used tissue samples which similarly found in the previous studies.[42][43] Differences' being small makes sense considering that the fact that biological soft tissues contain up to 80 percent water thus the refractive indices are close to the water so that their refractive index value differences are close to each other mostly. [31]

If the Figure 4.21 is analysed, all of these signal difference and the signal differences' being close to the simulated signal can be seen more obviously.

Before the comparison with the experimentally measured sample signals of the oral soft tissue samples, the reasonable assumption was obtaining small differences between simulated signals of the 5 biological samples by IFFT analysis using one known refractive index. After the analyse, it is shown that the assumption is consistent with the result.

These results are also promising for the future studies by indicating that with an upgraded and more sensitive THz-ATR time domain spectroscopy system, even the small refractive index differences between biological samples can be detected more accurately or used to differentiate infections.

CONCLUSION

A Yb:doped mode-locked fiber laser THz driven ATR-TDS system with bandwidth of roughly 0.3 THz is developed in this thesis for measurement of biolgocial soft tissues. 5 oral soft tissue samples obtained with permission from subjects with the assistance of the Faculty of Dentistry in Ankara University are used as biological test samples. These biological samples are carefully placed on to the ATR Si prism surface so as to be in full conttact. Due to the limitted bandwidth of the system and the nature of the time-domain waveforms it was difficult to exract the complex material paramees withhigh precision from the obteined measured data sets. In order to assess the complex refracive index of the biological samples an analysis routine is developed based on the obtained reference scan, i.e. without bological sample. By implementing Inverse Fourier Transformatio, THz ATR-TDS sample signals in time domain are simulated successfully using the estimated refractive index (water is used as the reference complex index since bilological tissues are mostly made up of water) for tissue samples and reference signal. Oral soft tissue sample signals obtained from the THz ATR-TDS measurements are compared to simulated sample signals in time domain and are shown to be in well agreement. Differences between the estimated refractive index and the actual value of the refractive indexes of the different samples appeared to be considerably small. A more detailed comparision analysis of these differences can lead to developing an estimation method for refractive index of biological medium since this thesis successfully shows that the THz ATR-TDS system is a great spectroscopy sytem for the optical analysis of biological materials

In future studies, the differencese between the estimated ATR sample signal in time domain and the experimentally acquired ATR sample signals of the oral soft tissues can be better aligned using iteratve methods to estimate the complex refracive

index. This can be achived by developing an algorithm using Python to obtain the complex and real parts of the refractive index. This possible study is promising because if changing the complex and real parts of the estimated refractive index can result in better fitting of experimental and simulated signals together than such methods can be utilized to ascertain the complex refracive index of the test sample.

REFERENCES

[1] F. Sizov, "Brief history of THz and IR technologies," *Semiconductor Physics, Quantum Electronics & Optoelectronics,* vol. 22, pp. 67-79, 2019.

[2] Y. Yu, "Measurement of Coating Thickness Based on Terahertz Time-Domain Spectroscopy (THz-TDS) Technology," p. 63.

[3] S. S W, C. J M, F. A J and E. Berry, "The interaction between Terahertz radiation and biological tissue," *Physics in Medicine and Biology,* vol. 46, no. 9, 2001.

[4] G. J. Wilmink and J. E. Grundt, "Invited Review Article: Current State of Research on Biological Effects of Terahertz Radiation," *Journal of Infrared, Milimeter, and Terahertz Waves,* vol. 32, no. 10, pp. 1074-1122, 2011.

[5] A. I. Nikitkina, P. Bikmulina, E. R. Gafarova, N. V. Kosheleva and Y. M. Efremov, "Terahertz radiation and the skin: a review," *Journal of Biomedical Optics,* vol. 26, 2021.

[6] H. F. Electronics, "Terahertz (thz) technology:an introduction and research update.," 2008.

[7] Inc, Eric R. Mueller, Coherent, "Terahertz Radiation Sources for Imaging and Sensing Applications," [Online]. Available: https://www.photonics.com/Articles/Terahertz_Radiation_Sources_for_Imaging_and/a27186.

[8] a. atalar, "TIME DOMAIN TERAHERTZ ATTENUATED TOTAL INTERNAL," 2021.

[9] J. R. Freeman, H. E. Beere and D. A. Ritchie, "Generation and Detection of Terahertz Radiation," in *Terahertz Spectroscopy and Imaging*, Berlin, Heidelberg, Springer, 2013, pp. 1-28.

[10] W. L. Chan, J. Deibel and D. M. Mittleman, "Imaging with terahertz radiation," vol. 70, no. 8, pp. 1325-1379, 2007.

[11] M. Tani, M. Hermann and K. Sakai, "Generation and detection of terahertz pulsed radiation with photoconductive antennas and its application to imaging," *Measurement Science and Technology,* vol. 13, no. 11, pp. 1739-1745, 2002.

[12] U. P. Jepsen, G. D. Cooke and M. Koch, "Terahertz spectroscopy and imaging modern techniques and applications," *Laser&Photonics Reviews,* vol. 5, no. 1, pp. 124-166, 2011.

[13] D. Grischkowsky, S. Keiding, V. M. Exter and C. Fattinger, "Far-infrared time-domain spectroscopy with terahertz beams of dielectrics and semiconductors," *JOSA B,* vol. 7, no. 10, pp. 2006-2015, 1990.

[14] X. Zhang, "Terahertz wave imaging: horizons and hurdles," *Physics in Medicine,* vol. 47, no. 21, p. 3667, 2002.

[15] J.-L. Coutaz, F. Garet and V. P. Wallace, Principles of Terahertz Time-Domain Spectroscopy, CRC Press, 2018.

[16] B. Karagöz, "PULSED THREE DIMENSIONAL THZ IMAGING," 2016.

[17] P. Y. Han, M. Tani, M. Usami, S. Kono, R. Kersting and X.-C. Zhang, "A direct comparison between terahertz time-domain spectroscopy and far-infrared Fourier transform spectroscopy," *Journal of Applied Physics,* vol. 89, no. 4, pp. 2357-2359, 2001.

[18] D. Holland, "Design, Construction, and Applications of a High-Resolution

Terahertz Time-Domain Spectrometer," p. 191.

[19] Y. Huang, R. Singh, L. Xie and Y. Ying, "Attenuated Total Reflection for Terahertz Modulation, Sensing, Spectroscopy and Imaging Applications: A Review," *Applied Sciences,* vol. 10, p. 4688, 2020.

[20] P. U. Jepsen and H. Merbold, "Terahertz reflection spectroscopy of aqueous nacl," *Journal of Infrared, Millimeter, and Terahertz Waves,* vol. 31, no. 4, pp. 430-440, 2010.

[21] E. Arik, H. Altan and O. Esentürk, "Dielectric properties of diesel and gasoline by terahertz spectroscopy," *Journal of Infrared, Millimeter, and Terahertz Waves,* vol. 35, no. 9, pp. 759-769, 2014.

[22] R. Ulbricht, E. Hendry, J. Shan, T. F. Heinz and M. Bonn, "Carrier Dynamics in Semiconductors studied with time-resolved terahertz spectroscopy," *Reviews of Modern Physics,* vol. 83, no. 2, p. 543, 2011.

[23] H. Hirori, K. Yamashita, M. Nagai and K. Tanaka, "Attenuated total reflection spectroscopy in time domain using terahertz coherent pulses," *Japanese journal of applied physics,* vol. 43, no. 10A, p. L1287, 2004.

[24] J. Gong and S. Krishnan, "Absorption Coefficient Alpha - an overview," ScienceDirect Topics, [Online]. Available: https://www.sciencedirect.com/topics/engineering/absorption-coefficient-alpha.

[25] M. Nagai, H. Yada, T. Arikawa and K. Tanaka, "Terahertz time-domain attenuated reflection spectroscopy in water and biological solution," *International journal of infrared and milimeter waves,* vol. 27, no. 4, pp. 505-515, 2006.

[26] M. Milosevic, Internal reflection and ATR spectroscopy, vol. 17, wiley,

2012.

[27] D. J. Griffiths, Introduction to electrodynamics, Prentice Hall New Jersey, 1962.

[28] "Optical and electronic properties of doped silicon from 0.1 to 2 THz," *Applied Physics Letters,* vol. 56, no. 17.

[29] U. Moller, G. D. Cooke, K. Tanaka and U. P. Jepsen, "Terahertz reflection spectroscopy of debye relaxation in polar liquids," *JOSA B,* vol. 26, no. 9, pp. A113-125, 2009.

[30] J. C. Lai, Y.-Y. Zhang, Z.-H. Li, H.-J. Jiang and A.-Z. He, "Complex refractive index measurement of biological tissues by attenuated total reflection ellipsometry," 2010.

[31] R. Pethig and D. Kell, "The passive electrical properties of biological systems: Their significance in physiology,biophysics and biotechnology," *Physics in medicine and biology,* 1987.

[32] A. Fitzgerald, E. Berry, N. Zinov'ev, G. Walker, M. Smith, and J. M. Chamberlain, "An introduction to medical imaging with coherent terahertz frequency radiation.," Physics in medicine and biology, vol. 47 7, pp. R67–84, 2002.

[33] Y. Sun, M. Y. Sy, Y.-X. J. Wang, A. T. Ahuja, Y.-T. Zhang, and E. PickwellMacPherson, "A promising diagnostic method: Terahertz pulsed imaging and spectroscopy," World journal of radiology, vol. 3, no. 3, p. 55, 2011.

[34] N. Harrick and K. Beckmann, "Internal reflection spectroscopy," in Characterization of Solid Surfaces, pp. 215–245, Springer, 1974.

[35] M. Milosevic, Internal reflection and ATR spectroscopy, vol. 176. John

Wiley & Sons, 2012.

[36] A. Wojdyla and G. Gallot, “Attenuated internal reflection terahertz imaging,” Optics Letters, vol. 38, no. 2, pp. 112–114, 2013.

[37] M. Van Exter and D. Grischkowsky, “Optical and electronic properties of doped 6765 silicon from 0.1 to 2 thz,” Applied Physics Letters, vol. 56, no. 17, pp. 1694– 1696, 1990.

[38] B. Karagöz, “Pulsed three dimensional thz imaging,” Master’s thesis, Middle East Technical University, 2016.

[39] H. Liu, Y. Wang, D. Xu, Z. Jiang, J. Li, L. Wu, C. Yan, L. Tang, Y. He, D. Yan, et al., “Optimization for vertically scanning terahertz attenuated total reflection imaging,” Optics express, vol. 26, no. 16, pp. 20744–20757, 2018.

[40] P. U. Jepsen, U. Møller, and H. Merbold, “Investigation of aqueous alcohol and sugar solutions with reflection terahertz time-domain spectroscopy,” Optics Express, vol. 15, no. 22, pp. 14717–14737, 2007.

[41] K. Sasaki, M. Mizuno, K. Wake, and S. Watanabe, “Monte carlo simulations of skin exposure to electromagnetic field from 10 ghz to 1 thz,” Physics in Medicine & Biology, vol. 62, no. 17, p. 6993, 2017.

[42] O. Cherkasova, M. Nazarov, and A. Shkurinov, “Noninvasive blood glucose monitoring in the terahertz frequency range,” Optical and Quantum Electronics, vol. 48, no. 3, p. 217, 2016.

[43] D. A. Newnham and P. F. Taday, “Pulsed terahertz attenuated total reflection spectroscopy,” Applied spectroscopy, vol. 62, no. 4, pp. 394–398, 2008.

[44] D. Grischkowsky, S. Keiding, M. Van Exter, and C. Fattinger, “Far-infrared time-domain spectroscopy with terahertz beams of dielectrics and semiconductors,” JOSA B, vol. 7, no. 10, pp. 2006–2015, 1990.

[45] J. B. Baxter and G. W. Guglietta, “Terahertz spectroscopy,” Analytical chemistry, vol. 83, no. 12, pp. 4342–4368, 2011.

[46] O. Svelto, D. C. Hanna, et al., Principles of lasers. Springer, 2010.

[47] E. Arik, H. Altan, and O. Esenturk, “Dielectric properties of diesel and gasoline by terahertz spectroscopy,” Journal of Infrared, Millimeter, and Terahertz Waves, vol. 35, no. 9, pp. 759–769, 2014.

[48] W. L. Chan, J. Deibel, and D. M. Mittleman, “Imaging with terahertz radiation,” Reports on progress in physics, vol. 70, no. 8, p. 1325, 2007.

[49] G.-S. Park, Y. H. Kim, H. Han, J. K. Han, J. Ahn, J.-H. Son, W.-Y. Park, and Y. U. Jeong, Convergence of Terahertz Sciences in Biomedical Systems. Springer, 2012.

[50] V. Apostolopoulos and M. Barnes, “Thz emitters based on the photo-dember effect,” Journal of Physics D: Applied Physics, vol. 47, no. 37, p. 374002, 2014.

[51] A. Nahata and T. F. Heinz, “Generation of subpicosecond electrical pulses by optical rectification,” Optics letters, vol. 23, no. 11, pp. 867–869, 1998.

APPENDIX

PYTHON CODE FOR DATA ANALYSIS

```
import matplotlib.pyplot as plt

import numpy as np

from scipy.fft import fft, fftfreq, fftshift,rfft,rfftfreq,irfft


x,y=np.loadtxt('AirRef.txt', usecols=[0,1], unpack=True)

n = len(x)

r = np.zeros((n, 2), float)

r[:,0] = x

r[:,1] = y



d = np.zeros((n,1),dtype=np.complex_)

d[:,0] = 1

N = 1000

# sample spacing

T = .1


rms = np.sqrt(np.mean(y**2))
```

```
yf = fft(y)

z = fftshift(fft(y))

xf = rfftfreq(N, T)[:N//2]

Eref = yf


angle = 51.6

deg2Rad = (np.pi/180)

cosine = np.cos(angle*deg2Rad)

sine = np.sin(angle*deg2Rad)

sineSquare = np.square(sine)


nprism = 3.42

nprismSquarePower = np.square(nprism)


nsample =1.4

nsampleSquarePower = np.square(nsample)


nair = 1

nairSquarePower = 1


a = nsampleSquarePower - nprismSquarePower * sineSquare
```

```
numerator1 = (nsampleSquarePower * cosine) - nprism *np.emath.sqrt(a)

denominator1 = (nsampleSquarePower * cosine) + nprism *np.emath.sqrt(a)

result1 = numerator1 / denominator1

b = nair - nprismSquarePower * sineSquare

numerator2 = (nairSquarePower * cosine) - nprism *np.emath.sqrt(a)

denominator2 = (nairSquarePower * cosine) + nprism *np.emath.sqrt(a)

result2 = numerator2 / denominator2

sample = Eref * (result1 / result2)

s = irfft(sample,N+1)


aira,airb=np.loadtxt('Air1.txt', usecols=[0,1], unpack=True)
n = len(aira)
```

```
l1 = np.zeros((n, 2), float)

l1[:,0] = aira

l1[:,1] = airb


airc,aird=np.loadtxt('Air2.txt', usecols=[0,1], unpack=True)

l2 = np.zeros((n, 2), float)

l2[:,0] = airc

l2[:,1] = aird


aire,airf=np.loadtxt('Air3.txt', usecols=[0,1], unpack=True)

l3 = np.zeros((n, 2), float)

l3[:,0] = aire

l3[:,1] = airf


airg,airh=np.loadtxt('Air4.txt', usecols=[0,1], unpack=True)

l4 = np.zeros((n, 2), float)

l4[:,0] = airg

l4[:,1] = airh


airj,airk=np.loadtxt('Air5.txt', usecols=[0,1], unpack=True)

l5 = np.zeros((n, 2), float)

l5[:,0] = airj
```

```
l5[:,1] = airk


plt.plot(aira, airb,label='Tissue 1')
plt.legend()
plt.style.use("seaborn-paper")
plt.xlabel('Time Delay(ps)')
plt.ylabel('THz Electric Field(arb.u.)')
plt.xlim(10,45)
plt.savefig('Tissue10.jpg', dpi = 2000 ,bbox_inches='tight')
plt.show()


plt.plot(aira, s)
plt.plot(aira, airb, ':')
plt.style.use("seaborn-paper")
plt.legend(('Sample', 'Tissue 1'))
plt.xlabel('Time Delay(ps)')
plt.ylabel('THz Electric Field(arb.u.)')
plt.xlim(10,45)
plt.savefig('Tissue1.jpg', dpi = 2000 ,bbox_inches='tight')
plt.show()


plt.plot(airc, aird,label='Tissue 2')
```

```
plt.legend()
plt.style.use("seaborn-paper")
plt.xlabel('Time Delay(ps)')
plt.ylabel('THz Electric Field(arb.u.)')
plt.xlim(10,45)
plt.savefig('Tissue20.jpg', dpi = 2000 ,bbox_inches='tight')
plt.show()

plt.plot(aira, s)
plt.plot(airc, aird, ':')
plt.style.use("seaborn-paper")
plt.legend(('Sample', 'Tissue 2'))
plt.xlabel('Time Delay(ps)')
plt.ylabel('THz Electric Field(arb.u.)')
plt.xlim(10,45)
plt.savefig('Tissue2.jpg', dpi = 2000 ,bbox_inches='tight')
plt.show()

plt.plot(aire, airf,label='Tissue 1')
plt.legend()
plt.style.use("seaborn-paper")
plt.xlabel('Time Delay(ps)')
```

```
plt.ylabel('THz Electric Field(arb.u.)')
plt.xlim(10,45)
plt.savefig('Tissue30.jpg', dpi = 2000 ,bbox_inches='tight')
plt.show()

plt.plot(aira, s)
plt.plot(aire, airf,':')
plt.style.use("seaborn-paper")
plt.legend(('Sample', 'Tissue 3'))
plt.xlabel('Time Delay(ps)')
plt.ylabel('THz Electric Field(arb.u.)')
plt.xlim(10,45)
plt.savefig('Tissue3.jpg', dpi = 2000 ,bbox_inches='tight')
plt.show()

plt.plot(airg, airh,label='Tissue 4')
plt.legend()
plt.style.use("seaborn-paper")
plt.xlabel('Time Delay(ps)')
plt.ylabel('THz Electric Field(arb.u.)')
plt.xlim(10,45)
plt.savefig('Tissue40.jpg', dpi = 2000 ,bbox_inches='tight')
```

```
plt.show()


plt.plot(aira, s)
plt.plot(airg, airh, ':')
plt.style.use("seaborn-paper")
plt.legend(('Sample', 'Tissue 4'))
plt.xlabel('Time Delay(ps)')
plt.ylabel('THz Electric Field(arb.u.)')
plt.xlim(10,45)
plt.savefig('Tissue4.jpg', dpi = 2000 ,bbox_inches='tight')
plt.show()


plt.plot(airj, airk,label='Tissue 5')
plt.legend()
plt.style.use("seaborn-paper")
plt.xlabel('Time Delay(ps)')
plt.ylabel('THz Electric Field(arb.u.)')
plt.xlim(10,45)
plt.savefig('Tissue50.jpg', dpi = 2000 ,bbox_inches='tight')
plt.show()


plt.plot(aira, s)
```

```
plt.plot(airj, airk, ':')

plt.style.use("seaborn-paper")

plt.legend(('Sample', 'Tissue 5'))

plt.xlabel('Time Delay(ps)')

plt.ylabel('THz Electric Field(arb.u.)')

plt.xlim(10,45)

plt.savefig('Tissue5.jpg', dpi = 2000 ,bbox_inches='tight')

plt.show()


plt.plot(aira, y)

plt.plot( aira, airb, ':')

plt.plot(airc, aird, ':')

plt.plot(aire, airf, ':')

plt.plot(airg, airh, ':')

plt.plot(airj, airk, ':')

plt.legend(('Reference', 'Sample1', 'Sample2', 'Sample3', 'Sample4', 'Sample5'))

plt.style.use("seaborn-paper")

plt.xlabel('Time Delay(ps)')

plt.ylabel('THz Electric Field(arb.u.)')

plt.xlim(10,45)

plt.savefig('TissueRefAlls.jpg', dpi = 2000 ,bbox_inches='tight')

plt.show()
```

```
plt.plot(aira, s)

plt.plot( aira, airb, ':')

plt.plot(airc, aird, ':')

plt.plot(aire, airf, ':')

plt.plot(airg, airh, ':')

plt.plot(airj, airk, ':')

plt.legend(('Sample', 'Sample1', 'Sample2', 'Sample3', 'Sample4', 'Sample5'))

plt.style.use("seaborn-paper")

plt.xlabel('Time Delay(ps)')

plt.ylabel('THz Electric Field(arb.u.)')

plt.xlim(10,45)

plt.savefig('TissueSampleAll.jpg', dpi = 2000 ,bbox_inches='tight')

plt.show()



plt.subplot(611)

plt.plot(aira, s)

plt.xlim(20,40)

plt.subplot(612)

plt.plot( aira, airb, ':')

plt.xlim(20,40)
```

```
plt.subplot(613)
plt.plot(airc, aird, ':')
plt.xlim(20,40)
plt.subplot(614)
plt.plot(aire, airf, ':')
plt.ylabel('THz Electric Field(arb.u.)')
plt.xlim(20,40)
plt.subplot(615)
plt.plot(airg, airh, ':')
plt.xlim(20,40)
plt.subplot(616)
plt.plot(airj, airk, ':')
plt.style.use("seaborn-paper")
plt.xlabel('Time Delay(ps)')
plt.xlim(20,40)
plt.savefig('TissueAllSeperatedZoomed.jpg', dpi = 2000 ,bbox_inches='tight')
plt.show()
```

```
plt.plot(aira, y)
plt.plot(aira, s, ':')
```

```
plt.style.use("seaborn-paper")
plt.legend(('Reference', 'Result'))
plt.xlabel('Time Delay(ps)')
plt.ylabel('THz Electric Field(arb.u.)')
plt.xlim(0,133)
plt.savefig('SampleResult.jpg', dpi = 2000 ,bbox_inches='tight')
plt.show()



plt.plot(aira, y)
plt.plot(aira, airb, ':')
plt.style.use("seaborn-paper")
plt.legend(('Reference', 'Tissue 1'))
plt.xlabel('Time Delay(ps)')
plt.ylabel('THz Electric Field(arb.u.)')
plt.xlim(0,133)
plt.savefig('Tissue1Ref.jpg', dpi = 2000 ,bbox_inches='tight')
plt.show()



plt.plot(aira, y)
plt.plot(airc, aird, ':')
```

```
plt.style.use("seaborn-paper")

plt.legend(('Reference', 'Tissue 2'))

plt.xlabel('Time Delay(ps)')

plt.ylabel('THz Electric Field(arb.u.)')

plt.xlim(0,133)

plt.savefig('Tissue2Ref.jpg', dpi = 2000 ,bbox_inches='tight')

plt.show()


plt.plot(aira, y)

plt.plot(aire, airf,':')

plt.style.use("seaborn-paper")

plt.legend(('Reference', 'Tissue 3'))

plt.xlabel('Time Delay(ps)')

plt.ylabel('THz Electric Field(arb.u.)')

plt.xlim(0,133)

plt.savefig('Tissue3Ref.jpg', dpi = 2000 ,bbox_inches='tight')

plt.show()


plt.plot(aira, y)

plt.plot(airg, airh, ':')

plt.style.use("seaborn-paper")

plt.legend(('Reference', 'Tissue 4'))
```

```
plt.xlabel('Time Delay(ps)')

plt.ylabel('THz Electric Field(arb.u.)')

plt.xlim(0,133)

plt.savefig('Tissue4Ref.jpg', dpi = 2000 ,bbox_inches='tight')

plt.show()


plt.plot(aira, y)

plt.plot(airj, airk, ':')

plt.style.use("seaborn-paper")

plt.legend(('Reference', 'Tissue 5'))

plt.xlabel('Time Delay(ps)')

plt.ylabel('THz Electric Field(arb.u.)')

plt.xlim(0,133)

plt.savefig('Tissue5Ref.jpg', dpi = 2000 ,bbox_inches='tight')

plt.show()
```